Fire performance on steel-reinforced concrete-filled steel tubular columns with fire protection

Wen-Jing Mao[a,b], Wen-Da Wang[a,b,*], Kan Zhou[c]

[a] *School of Civil Engineering, Lanzhou University of Technology, Lanzhou 730050, PR China*

[b] *Western Center of Disaster Mitigation in Civil Engineering of Ministry of Education, Lanzhou University of Technology, Lanzhou 730050, PR China*

[c] *School of Built Environment, Engineering and Computing, Leeds Beckett University, City Campus, Leeds, LS1 3HE, UK*

Abstract: Steel-reinforced concrete-filled steel tube (SRCFST) is widely used as an innovative composite structure to provide better performance in construction. This study focuses on comprehensive experimental and numerical investigations of the fire performance of SRCFST columns with fire protection under the ISO-834 standard fire test procedures. The fire resistance tests were conducted on eight SRCFST columns with various thicknesses of fire resistive coating. The fire test results, including the thermal conductivity of protection material, failure modes, temperature evolution in time, axial and lateral deformation curves, and fire resistance were reported in detail. The results demonstrated that fire protection delayed the degradation of bending stiffness and significantly increased the fire resistance. Further comparisons of fire resistance between SRCFST columns with and without fire protection indicated that the fire resistance of SRCFST column with protection thickness of 12 mm is 3.32 times higher than that of that without fire protection under an equal load level. A sequentially coupled thermal-stress finite element (FE) analysis model was develped and validated against the tested results. The measured thicknesses of fire resistive coating were compared with the predicted results to evaluate the applicatibility of the existing design method

of concrete-filled steel tubular (CFST) columns to SRCFST columns with thick fire-resistive coating. The results indicated that the current design method should be adjusted or modified further to provide safe and accurate predictions of the thickness of fire protection for SRCFST columns.

Keywords: steel-reinforced concrete-filled steel tubular columns; fire protection; fire resistance; fire resistive coating; finite element (FE) analysis

*Corresponding author: at School of Civil Engineering, Lanzhou University of Technology, PR China

E-mail: wangwd@lut.edu.cn (W.-D. Wang).

Tel./fax: +86 931 2350533;

Wen-Da Wang, Professor of School of Civil Engineering, Lanzhou University of Technology, China

1. Introduction

Composite structures are generally composed of two or more materials. These are used widely in advanced structures such as concrete-filled steel tube (CFST), steel-reinforced concrete (SRC), and fiber-reinforced polymer (FPR) confined concrete. The high performance of building structural materials and building structures is known to be one of the important development directions of composite structure. Various new types of composite structural components such as FPR-confined CFST, concrete-filled double skin steel tube (CFDST), recycled CFST, and steel-reinforced concrete-filled steel tube (SRCFST) have emerged to provide better performance in various scenarios and aspects.

Branching from conventional CFST, SRCFST can be obtained by inserting profiled steel in concrete [1]. The concept of a hollow section filled with concrete and profiled steel for SRCFST has several advantages serving as vertical load bearing members. This is owing to the collaboration among the concrete, steel tube, and profiled steel [2]. Extensive experimental and numerical studies on the static behavior and mechanical characteristics of SRCFST members at ambient temperature have been conducted in the past decades [3-10]. It was revealed that profiled steel suppressed and delayed the development of cracks in concrete and consequently, improved the ductility of columns. Meanwhile, the concrete around the profiled steel provided confinement for it. This resulted in a slower degradation of stiffness. Moreover, the inserted profiled steel could function as a crucial component to improve the bearing capacity of SRCFST columns. Consequently, SRCFST columns exhibited better mechanical properties than CFST owing to a specific combination of three components, *i.e*., steel tube, concrete, and profiled steel. However, this also results in the complexity of its mechanical properties.

Extensive experiments and numerical analyses have been performed to study the fire performance of CFST columns [11]. These facts were also demonstrated in reviews [12-22]. However, present reviews of literature reveal that investigation on the fire resistance of SRCFST columns is limited. Chu et al. [23] conducted 10 fire tests on CFST columns filled with self-compacting concrete

and embedded by profiles (tube and H section). A numerical analysis was also performed to validate the test data. The fire performance of steel-reinforced concrete-filled stainless-steel tubular (SRCFSST) columns (e.g., temperature distribution, failure modes, and internal force distribution) was examined by Tan et al. [24] using the FE analysis. Espinos et al. [25] compared the fire performance of CFST columns with inner steel profiles including HEB profiles, steel core profiles, and circular hollow sections (CHS). In addition, studies on the fire behavior of CFST columns with solid steel core are available [26-29]. Furthermore, the post-fire behavior of SRCFST columns was investigated experimentally and numerically. The formulas for predicting the residual strength of SRCFST columns are available [30, 31].

The previous experimental data indicate that SRCFST columns without fire protection under common load level cannot achieve fire resistance rating in the class I category (180 min). Considering this, it is necessary to apply fire protection to SRCFST columns in practice. Various types of passive fire protection materials, including sprayed materials, plaster board, and intumescent coatings, have been applied in steel and composite structures. Intumescent coatings are a separate category of materials which although originally applied in thin layers. During the last decades, extensive investigations were performed to assess the fire resistance of intumescent coatings as an insulating material to steel structures [32-34] and fibre reinforced polymer (FRP) profiles [35, 36]. In addition, super absorbent polymer (SAP) materials are also used to achieve fire protection of steel structures by heat consumption during fire exposure. As a new protection mechanism, the fire performance of cold-formed steel walls protected by super absorbent polymers were experimentally investigated by Chen et al. [37] and Liu et al. [38].

Among different fire protection materials, thick fire-resistive coating is currently popular used in commercial steel buildings due to low price, good fire behavior and advantage of workability. It can easily protect complicated beam-column junctions, trusses and secondary element. At present, extensive literatures reported the research findings and design methods on fire resistance of CFST columns and steel structures protected by thick fire-resistive coating [39-41]. Several codes

recommended by various countries and design methods proposed by working groups are in use nowadays to estimate the fire resistance of CFST columns and steel structures. However, limited investigation has been performed on the fire performance of SRCFST columns with fire protection. The fire performance evaluation of SRCFST columns with thick fire-resistive coating is still missed. This is presumably because (1) the study on the fire response of SRCFST structures is in its infancy, and (2) there are limitations on the testing setups and fire tests are expensive. Moreover, the available design methods for CFST columns and steel structures do not explicitly present the applicability to SRCFST columns with fire-resistive coating; this inspired the present study. The intent was to further investigate the fire performance of SRCFST columns with fire-resistive coating and verify the applicability of existing design methods.

Considering the limited number of studies on SRCFST columns with fire resistive coating, eight SRCFST columns with thick fire-resistive coating were tested under the ISO-834 standard fire to address the data inadequacy. The fire performance of SRCFST columns with fire resistive coating, including failure mode, temperature distribution of cross-section, fire resistance, and failure process, were analyzed and discussed in detail. The effects of fire protection and its thickness on fire performance were discussed and compared with bare SRCFST columns based on previous results. Finally, the protection thicknesses of fire resistive coating were predicted to evaluate the applicability of the design methods for CFST columns as prescribed by GB 50936-2014 [42], BS 5950-8: 2003 [43], and Han et al. [44].

2. Experimental program

2.1 General description

In the testing program, eight SRCFST columns were designed and prepared in accordance with GB 50936-2014. Four circular hollow sections (CHS 325 × 6) and four square hollow sections (SHS 300 × 300 × 5.5) were used. A cruciform steel section was designed for the SRCFST column specimens. Two shapes were used for the steel tubes: labelled *A* for circular section and *B* for square section. Two initial loading eccentricities (50 mm and 80 mm) were considered for the circular cross-

sectioned specimen. The geometric dimensions and detailed parameters are presented in Table 1. The SRCFST specimens were labeled to indicate different parameters, e.g., CSUP-P50-50-1. The cross-section ID is indicated in the first phrase ("CS" and "SS" denote circular and square hollow sections, respectively). This is followed by "U" and "P" representing uniform fire exposure and SRCFST specimens with fire protection, respectively. The loading mode is indicated by "Z" (denoting concentric loading) or "P50/80" (denoting loading eccentricity). This is followed by the load level applied during the fire tests.

Eight SRCFST column specimens were fabricated in the same batch with SRCFST column specimens without fire protection. The details are described in Ref. [45]. Two roller supports with a total length of 940 mm were used to simulate the pinned-pinned condition. Thus, the effective length of the SRCFST column specimen was 4750 mm (see Fig.1). To realize initial loading eccentricities of 50 mm and 80 mm, end plates of different sizes (each with corresponding bolt-holes) were used to connect with the loading plate of the roller support. The detailed dimensions and end connections of the SRCFST column specimen are exhibited in Figs. 1 and 2. For a column with an initial loading eccentricity of 50 mm, the end plates with a side length of 600 mm were installed in alignment with the specimen. The centroid of the specimen was located 50 mm away from the central axis of the bearing support. In addition, an end plate with dimensions of 660 × 600 mm was designed. Its central axis was located 50 mm from the column center and 30 mm away from the central axis of the bearing support (Fig. 2(b)). Therefore, the initial loading eccentricity of 80 mm between the SRCFST column specimens and bearing support was considered and spaced.

Two-layer thermocouples located at mid-height (labelled as T1–T6) and 1 m below the mid-height (labelled as T7–T12) of the column were pre-embedded in the SRCFST column specimens to monitor the temperature. Six Type-K thermocouples with a diameter of 3 mm were arranged at identical coordinates in each layer. The position of the thermocouples was specified as shown in Fig. 2 (d)–(e).

A thick fire-resistive coating was used as fire protection for the SRCFST column specimen. It

was sprayed uniformly on the outside surface of the steel tube during specimen curing. To ensure a smooth and uniform coating, the fire resistive coating was sprayed in layers until the target thickness was attained.

2.2 Material testing

A tensile test was conducted to determine the material properties of steel (including the steel tube and welded profiled steel) at ambient temperature. The slats were cut for coupons. Three test coupons were prepared for each type of steel, forming a group. The key material properties including Young's modulus (E_s), yield strength (f_y), ultimate tensile strength (f_u), Poisson's ratio (μ_s), and elongation (δ_{10}) on an average are listed in Table 2.

Concretes of grades C50 and C70 were produced using 42.5# ordinary Portland cement, limestone gravel with an aggregate size of 5–20 mm, and fine aggregate with a fineness modulus of 2.9. The mix design for the C50 concrete used for casting the SRCFST column specimens and C70 concrete used for repairing the top of the columns are presented in Table 3. Test cubes were cast and cured in conjunction with SRCFST column specimens under an identical condition. The average cube compressive strength was measured to be 47.4 MPa (28 day) and 64.4 MPa (test day).

2.3 Measurement of thermal conductivity of thick fire-resistive coating

Thermal conductivity is the most important parameter defining the performance of an appropriate fire protection material. The temperature of a fire resistive coating varies from the normal temperature to 1200 °C during fire exposure. This causes a variation in conductivity coefficient with temperature. To simplify the calculation, the equivalent conductivity coefficient is employed to comprehensively reflect the actual performance of the fire resistive coating according to DG/TJ 08-008-2017 [46]. The equivalent conductivity coefficient test was conducted under the standard fire to determine the heat insulation performance of the thick fire-resistive coating used in this study.

2.3.1 Test preparation

Fire resistive coating of the model NH(FTH-1) was used. Its properties satisfy the requirements specified in code [47]. Three steel plates with a thickness of 16 mm and dimensions of 300 × 300 mm

were prepared as test coupons. Two K-type thermocouples, each with the tips located in the middle thickness of the plate, were mounted on the steel plate to measure the temperature. The dimensions of the test coupons and detailed positions of the thermocouples are indicated in Fig.3, where d_i is the thickness of the fire resistive coating. The fire resistive coating with a thickness of 20 ± 2 mm were sprayed on all the surfaces of the steel plate in a number of layers after rust removal, according to DG/TJ 08-008-2017[46].

A horizontal fire furnace test system was used to determine the equivalent conductivity coefficient, as displayed in Fig. 4. Two craters and two thermocouples were used to control and minor the furnace temperature. The test coupons were suspended and positioned in the fire furnace chamber with inner dimensions of 4 × 3 × 1.5 m (see Fig. 5(a)). The test was terminated when (1) the average temperature of the steel plate attained 540 °C or (2) the fire duration attained 3 h.

2.3.2 Test procedure and results

The fire test was terminated when the temperature of all the measurement points attained 540 ℃ (approximately 1 h). The conditions of the coupons after the fire test are shown in Fig. 5(b). The fire resistive coating cracked and shed partially after cooling. Fig. 6 shows the measured temperature of the thermocouple inner test coupons and fire furnace. It can be observed that the furnace temperature nearly coincided with the ISO-834 standard curve.

The equivalent thermal conductivity λ_i of the protection material is calculated according to DG/TJ 08-008-2017 [46] as follows:

$$\lambda_i = \frac{d_i}{\frac{5\times10^{-5}}{(\frac{T_s - T_{s0}}{t_0} + 0.2)^2 - 0.044} \times \frac{2}{d}} \tag{1}$$

where λ_i (W/(m·K)) is the equivalent thermal conductivity of the fire-resistant materials; d_i (m) and d(m) are the thicknesses of the fire resistive coating and steel plate, respectively; T_{s0} is the temperature of the steel plate before heating starts and is considered as 20 °C; T_s is the internal temperature of the test coupons at t (s) and is considered as 540 °C; and t_0 (s) is the time for the average temperature of

the test coupons to attain 540 °C.

Thus, the equivalent thermal conductivity of the three test coupons were 0.358 W/(m·K), 0.369 W/(m·K), and 0.347 W/(m·K). The average equivalent thermal conductivity for the fire resistive coating used in this study was 0.359 W/(m·K).

2.4 Fire tests

Fire tests were conducted on the SRCFST column specimens with thick fire-resistive coating to investigate the fire resistance performance under the ISO-834 [48] standard fire. A displacement gauge was mounted vertically at the upper rigid plate of the top roller support to obtain the vertical displacement. Simultaneously, a displacement gauge was positioned horizontally at the mid-height of the column to record the lateral deflection of specimens. Detailed information is presented in Ref. [45]. The instrumentation for the fire tests is displayed in Fig. 7 (the specimens in this test were protected with fire resistive coating).

A pre-load of 300–500 kN was applied before heating started, to close any likely gap. Prior to fire exposure, the compressive load was applied in steps of $N_F/10$ until the target load listed in Table 1 was attained. The data were recorded as the initial displacement after target load and stabilization. Subsequently, the fire furnace was preheated manually until a temperature close to that prescribed by ISO-834 was attained. The SRCFST column specimens with stable applied load were heated continually under standard fire. The fire test was terminated after failure was detected.

3. Test results

3.1 Fire tests

The failure of SRCFST columns was accompanied by a loud noise caused by the crushing of concrete. The typical failure modes of SRCFST columns with fire protection are presented in Figs. 8-9. For simplicity, Fig. 8(c) shows the arrangement of specimens inside the furnace, with the fixed part of furnace as west and the position mounted lateral gauges as south.

The global instability failure was ordinarily accompanied by the lateral deflection of columns as observed from the post-fire examination of SRCFST specimens. The cracking and shedding of the

protection material could be observed clearly at the mid-height of the columns and near the maximum lateral deflection. It was more severe at the compression side. The protection materials of four circular SRCFST column specimens were damaged, but no large area of spalling was observed. However, the steel tube at the middle area of four square SRCFST columns were exposed entirely owing to the severe exfoliation of the protection materials (see Fig. 9), although the shrinkage of the protection material during the cooling had possibly aggravated the cracking and shedding of the fire resistive coating. Obvious local buckling of the steel tube was observed on the compression side of CSUP-P50-50-1 (see Fig. 8(b)) owing to the stiffness degradation of the steel tube.

The fire resistive coating was removed manually for a clear view of the failure modes of the SRCFST columns (see Fig. 10). Note that the photograph of SSUP-Z-80-4 in Fig. 10 has been mirrored to effectively compare the lateral deformation among eight SRCFST specimens. All the specimens exhibited global failure accompanied by lateral deflection. No local buckling was observed in the three circular SRCFST specimens apart from CSUP-P50-50-1. This is because the columns under a larger load level are more likely to attain the ultimate level of stress-induced strain, resulting in fail earlier caused by a globe buckling. In addition, the local buckling was more severe for the square specimens. These featured waved bulges along the height of the columns. This was because columns under eccentric load are more sensitive to global buckling. Meanwhile, the reinforcement provided by a circular steel tube to the inner concrete is more uniform than that provided by a square steel tube.

To examine the inner states in detail, the steel tubes of the SRCFST column specimens were cut and removed manually to expose the concrete. The failure modes of concrete are presented in Fig. 11, taking the specimens with higher load level as examples. The concrete of the circular SRCFST displayed high integrity, indicating the high restraint provided by the circular steel tube to the concrete (see Fig. 11(a)–(b)). For CSUP-P80-70-4, it can be observed that the concrete fragment in the tension side was near the maximum lateral deformation. This was different from that for CSUP-P80-70-3. The following could have been the reasons: (i) the concrete of CSUP-P80-70-4 shared more load

compared with that of CSUP-P80-70-3, owing to the higher temperature of the steel tube of CSUP-P80-70-4, and (ii) the concrete in the tension side was severely pulled apart under the eccentric load and high load level. For the square SRCFST specimen, significant concrete crushing was observed at the maximum position of the lateral deflection. Transverse cracks and several small longitudinal cracks were observed at the tension side. The transverse cracks were only distributed within 500 mm and were caused by partial concrete shedding.

By chiseling out the concrete to expose the profiled steel, it could be observed that the lateral deflection of the profiled steel was consistent with that of the column. However, unlike the bare SRCFST specimen, local buckling was not observed for the flange of the profiled steel as presented in Fig. 11(c), although the SRCFST specimens with fire protection sustained a higher load level. The reason is that the protected SRCFST specimens had higher bending stiffness compared with the bare SRCFST specimens for an equal heating time. This was caused by the lower temperature of the entire cross-section of the protected SRCFST specimens.

3.2 Temperature evolution

Twenty-five thermocouples (TC1–TC25) were pre-embedded in the interior walls of the furnace. These were used to monitor and control the furnace temperature. The temperature evolution of TC1–TC10 was compared with the ISO-834 standard curve considering CSUP-P50-50-1 as an example. It was consistent with the standard curve, as shown in Fig. 12(a). TC11–TC25 are omitted in the figure because of the similar furnace temperature obtained by the 25 thermocouples. Fig. 12(b) shows the average furnace temperature of the SRCFST specimens during the fire.

The temperature evolution recorded at the measurement point (illustrated in Fig.2) of the SRCFST specimens during the fire test are presented in Fig. 13. A few thermocouples failed during the fire exposure, thereby resulting in data loss and irregular variation. The temperature data attained from the steel tube of CSUP-P50-50-1 are presented in Fig. 13 (a). Compared with the furnace temperature, the increase in temperature followed the basic form of the standard fire, although at a lower rate. Furthermore, the maximum temperature was below 600 °C. This was owing to the

influence of the fire resistive coating. Fig. 13 (a) also shows the temperature evolution at the measurement point of concrete and profiled steel, which indicates lagging the temperature increase of concrete and profiled.

The temperature obtained from profiled steel and concrete were significantly close during the entire fire test. This phenomenon is related to the thermal inertia of the concrete, thermal insulation of the fire resistive coating, thermal contact resistance at the interface between fire resistive coating and steel tube, and that at the interface between steel tube and concrete. Meanwhile, the concrete as a material protecting from the temperature increase delayed the increase in temperature of profiled steel. The comparison with the temperature results of the two-layer thermocouples shown in Fig. 1 indicates that the temperature was almost uniformly distributed along the longitudinal of SRCFST columns. The T3 and T9 (located in the flange of the profiled steel) of CSUP-P50-50-1 captured the saltation in the temperature evolution. These indicated that concrete cracks were starting to appear around the profiled steel and caused contact fault. Similar visual evolution in time of the temperature of other specimens are presented in Figs. 13(b)–(c). Furthermore, an abrupt temperature variation was observed at the measurement point of the steel tube. It was particularly evident in CSUP-P50-70-2, CSUP-P80-70-3, CSUP-P80-70-4, and SSUP-Z-80-3. This indicated that the steel tube around thermocouples were completely exposed in the fire starting from the abrupt point, and lost the protection provided by the fire resistive coating.

Furthermore, the obtained temperature evolution in time of the SRCFST column specimens with fire resistive coating under the ISO-834 standard fire can be characterized as follows: (1) An increasingly steep temperature gradient developed in the steel tube from the start of the fire test, whereas the lagging temperature in the concrete and profile resulted in an increasing temperature gradient in the radial direction of cross-section. (2) An evident plateau or gradual increase in the temperature curves of the steel tube was observed at approximately 200 °C except for SSUP-Z-80-4. This phenomenon could have resulted from the evaporation of free water from the fire resistive coating. The fire resistive coating used in the fire test contained moisture. When the temperature

within the material approached 100 °C, further heat input vaporized the free moisture rather than increasing the temperature of the materials [49]. This caused a "dwell" or delay in the increase in the temperature of the protected steel section. An example of the temperature increase in a protected steel tube is shown in Fig. 14. The duration of the plateau is defined as delay time t_v:

$$t_v = \frac{c\rho_p d_p^2}{5\lambda_p} \tag{2}$$

where c is the percentage of moisture content in the material, ρ_p is the density of the insulation, λ_p is the thermal conductivity of the fire protective material, and d_p is the thickness of the protection.

The comparison between the tested delay time and calculated data are summarized in Fig. 15. The deviations in t_v were not significant. (3) The temperature of the concrete and profiled steel increased gradually owing to the re-onset of the rapid increase in temperature of the steel tube. The longitudinal temperature of the steel tube continued to develop in accordance with the stable temperature deviation. When the temperature of concrete was approximately 100 °C, the migration and evaporation of the free water in the concrete resulted in the formation of a plateau in the temperature curves of concrete. It was particularly significant in CSUP-P50-70-2 and SSUP-Z-70-2. (4) An increasingly steep or abrupt variation in temperature of the steel tube can be observed until the end of the fire test. At the end of the test, a temperature deviation larger than 100 °C existed between two layers of thermocouples at the steel tube, except for CSUP-P50-50-1. The temperature data indicated the protective effect of the fire resistive coating from the increasing temperature.

3.3 Deformation of SRCFST columns during the fire

The deformation results of the SRCFST column specimens, including the axial deformation plotted on the left axis and lateral displacement plotted on the right axis, are presented in Figs. 16-17. Herein, the deformation induced by loading at ambient temperature is removed. For the axial deformation curves, the tension is considered as positive. However, for lateral displacement, deflection toward the displacement gauges is taken as negative and vice versa. Note that the displacement gauges were mounted at identical positions for each specimen. The lateral displacement

versus time curves of the partial specimens (CSUP-P50-50-1, SSUP-Z-60-1, and SSUP-Z-70-2) are not shown in the figures owing to the measurement of failure during the fire test.

The axial deformation of SRCFST was influenced by the combined expansion induced by the temperature and compressive deformation owing to the load. Although the temperature deviations between steel tube and profiled steel resulted in different thermal expansion, the deformation of the profiled steel was accordance with steel tube in axial because the steel tube and profiled steel were welded to the top and bottom end plates (the details are provided in Ref. [45]). The expansion of the steel tube elevated the top end plate in the early stage and resulted in detachment at the interface between concrete and end plate. This occurred primarily because of the temperature lag and low thermal expansion of concrete. Thus, most of the load could be carried by the steel tube and profiled steel at the initial stage of fire exposure. Subsequently, the stiffness of the steel tube degraded as the temperature increased, and the concrete regained contact with the end plate. The load shares of three components were redistributed toward the interior.

Fig. 16 shows the deformation results of the circular SRCFST specimens with eccentric loading. These featured a similar visible bending line owing to the predictability of the deflection direction before the test. Thus, the lateral deformation on the compression side was measured. The similarities of both axial and lateral deformation evolution of four specimens are illustrated considering CSUP-P50-70-2 as an example. The axial deformation increased gradually from the start of heating to 48 min, whereas the lateral deformation decreased in contact rate owing to the thermal expansion in the radial direction. The peak expansion was attained at 46 min and remained until 48 min. At this instant, the temperature obtained by the measurement point in the steel tube was 300-345 °C owing to the protection by the fire resistive coating. This had negligible effect on the strength of the steel tube, although the plasticity decreased according to [50]. Thereafter, from 48 min to 78 min, the axial deformation decreased, whereas the lateral deformation stabilized. This occurred because of the local buckling of the steel tube. Eventually, the lateral deflection began to increase significantly, whereas the axial deformation decreased rapidly after 78 min until failure occurred.

The peak expansion of CSUP-P50-70-2 was reduced significantly by a high load level of 0.7. This resulted in a maximum expansion of 1.01 mm, which was 73% shorter than that of CSUP-P50-50-1 under a common load level of 0.5. In addition, the magnitude of the peak expansion was also related to the thickness of the fire resistive coating. It decreased with an increase in the thickness. Specimen CSUP-P80-70-3 with a fire resistive coating of 14 mm attained a peak expansion of 2.03 mm. For CSUP-P80-70-4 under an identical load level, the magnitude of the peak expansion reduced by a thinner fire protection of 12 mm and resulted in a peak expansion of 0.29 mm. In addition, there were common characteristics in the peak expansion of SSUP-Z-80-3 and SSUP-Z-80-4 (see Fig. 17). This is because the SRCFST specimen with a thicker fire resistive coating was heated at a smaller rate, which resulted in less degradation of stiffness and strength. Therefore, it requires more time for expansion induced by heat to offset the contraction induced by the load.

Fig. 17 displays the recorded deformation of the axially loaded SRCFST specimens with square cross-section. SSUP-Z-80-4 deflected to the side away from the displacement gauge owing to the unpreventable initial imperfection, which was different from the other specimens. Thus, only the lateral deformation of SSUP-Z-80-4 on the tension side was measured. It is presented in Fig. 17(b). SSUP-Z-80-4 expanded with a minor rate at the beginning of heating until 61 min, whereas the lateral displacement decreased gradually with an abrupt decrease at 30 min. This indicated that the bending stiffness of the steel tube decreased, with the load redistributing among each component simultaneously. Subsequently, the lateral deformation continued to decrease in contact rate, whereas the axial expansion attained its peak, with a stabilized continuation from 61 min to 63 min. Both lateral and axial deformations significantly decreased abruptly from 82 min until the fire resistance limit.

The axial deformation curves for the tested SRCFST column specimens can be divided into three stages: an expansion stage at the beginning of fire exposure, a contraction stage caused by axial compressive deformation exceeding thermal expansion until failure, and fast runaway failure (see Fig. 16(a)). Meanwhile, it can be observed that all the SRCFST specimens with fire resistive coating were

destroyed abruptly without forewarning, indicating low ductility of the SRCFST column specimens with fire resistive coating.

3.4 Discussion on the fire resistance

3.4.1 Influence of load ratio

A discussion on the influences of the load ratio on the fire resistance of SRCFST columns is presented in this subsection. It is generally considered that the load level is among the significant factors affecting the fire resistance of column structures. The fire resistance decreased with the increase in load ratio, as illustrated in Fig. 18. For the protected square specimens with a thickness of 17 mm, the fire resistance reduced by 19% with an increase in the load level from 0.6 (SSUP-Z-60-1) to 0.8 (SSUP-Z-80-4). Similarly, an increase in the load level from 0.7 to 0.8 caused a reduction of 21% for the protected square specimens with a thickness of 12 mm.

3.4.2 Influence of eccentricity

The increase in eccentricity reduced the fire resistance of the SRCFST column specimens, as shown in Fig. 19. For a circular SRCFST specimen with an equal load level, the fire resistance reduced from 83 min in CSUP-P50-70-2 to 63 min in CSUP-P50-70-3 with an increase in the eccentricity from 50 mm to 80 mm. The second-order moment had significant effects on the column with a higher slenderness ratio. Thus, an increasing eccentricity caused the earlier instability failure of the column.

3.4.3 Influence of fire protection

The tested results for different thicknesses of fire protection material on circular SRCFST columns with an eccentricity of 80 mm are presented in conjunction with the results for the square columns under axial compression (see Fig. 20). For a square SRCFST specimen with an equal load level, the fire resistance varied from 62 min to 83 min (an increase of 25.3%) as the thickness of fire resistive coating increased from 12 mm (SSUP-Z-80-3) to 17 mm (SSUP-Z-80-4). Similar results were observed for the circular SRCFST column specimens.

The fire resistance of the SRCFST columns without fire protection were tested in the review [45]

and compared with the results obtained in this study (see Fig. 21). The fire resistance increased from 31 min to 103 min (an increase of 2.32 times) when the cross-section of CSU-P50-40 was protected by fire resistive coating with a thickness of 12 mm, although the load level varied from 0.4 to 0.5. Through the protection with a thickness of 14 mm, the fire resistance of CSU-P50-40 increased from 31 min to 83 min in CSUP-P50-70-2 with a load level of 0.7 (an increase of 1.68 times). For a benchmark study, the fire resistance obtained from the tests performed on unprotected SRCFST columns was compared with that obtained in this. This is summarized in Table 4. Note that the specimens were divided into three types in terms of cross-sectional form and eccentricity. The bare specimens with a common load level in each group were set as the standard specimens and were marked. It can be observed that the fire resistive coating significantly contributed to the improvement of fire resistance. The increase in the thickness of fire protection material can help increase its fire resistance. It is an important means for satisfying the fire-resistance rate in the fire resistance design of SRCFST columns.

4. Numerical modelling

4.1 General

The finite element (FE) analysis model was developed using the ABAQUS software. Detailed modeling procedures for the test specimens are described in this section. Thereafter, the temperature distribution using different thermal properties was predicted and compared. Furthermore, the developed FE models were validated based on the test results. In addition, the influence of the thermal resistance of the protective material on the temperature distribution and fire resistance were analyzed.

4.2 Finite element analysis (FEA) model for temperature field

The three-dimensional thermal FE model was first established using the eight-node liner brick heat-transfer element DC3D8. Thermal convection and thermal radiation were set in the model to consider the heat transfer from the atmosphere to the column. The thermal convection coefficient and thermal emissivity coefficient were taken as 25 W/(m^2·°C) and 0.7, respectively, according to EC 4 [51]. The Stefan–Boltzmann constant is 5.67×10^{-8} W/(m^2·k^4). For simplicity, the initial temperature

was taken as 20 °C. The end plate was omitted in the heat transfer analysis. The ISO-834 standard curve was used as a thermal load. The thermal contact resistance of the interface between steel tube and concrete was taken into account in the calculation of temperature. It was considered as 0.01 (m^2·°C)/W [27].

The thermal property of steel and concrete are not identical in the present fire design. For comparison, three types of thermal properties (thermal properties proposed by Lie [50] and those recommended in EC4 [51] and BS 5950-8:2003 [43]) were used to calculate the temperature distribution. These were labelled FE-1, FE-2, and FE-3, respectively. The temperature-time response of the cross-section was affected significantly by the moisture content of concrete. For the specific heat of concrete proposed by Lie [50], the moisture content of concrete was assumed to be 5% by weight, and the expression was modified. Nevertheless, a moisture content of 4% was assumed for concrete in the calculation employed by EC4 and BS 5950-8:2003.

The measured temperature of the SRCFST columns without fire protection at the end of fire exposure was compared with the predicted results. This is reported in Table 5. For the critical temperature at the measurement point of the steel tube, the values calculated using the above three types of thermal properties varied marginally. Calculated values were over-predicted by approximately 150 °C for the specimens under a load level of 0.4. The predicted critical temperature of the remaining specimens was consistent with the measured results. For the maximum temperature at the measurement point of concrete, the values calculated by the three types of thermal properties differed significantly. Quantitative and synthetic assessments of temperature were conducted through a comparison with the predicted and measured temperatures (see Table 5). The results predicted using the thermal properties proposed by Lie were conservative, whereas the temperature determined using the thermal properties given in EC4 and BS 5950-8:2003 were over-predicted by 2.5% and 5.7%, respectively. The evaluation results revealed that the thermal properties recommended in EC4 yielded more accurate and consistent temperature predictions. Therefore, the thermal properties of steel and concrete in EC4 were adopted in the FE model for the temperature field.

4.3 Effect of thermal resistance of fire resistive coating

A significantly thick fire protection coating would have a certain thermal capacity. This would reduce the heat flux to the steel section. Thus, the thermal resistance is a significant parameter for determining the heat flow through a thin fire-protective material into a steel section. It can be expressed by *Eq.*(3). Here, R is the thermal resistance of the fire protection. The influences of the thermal resistance of the protection material on the temperature development at the surface of a steel tube were analyzed.

$$R = \frac{d_i}{\lambda_p} \tag{3}$$

The predicted temperature of the steel tube and concrete were compared with the test results. This is plotted in Fig.22. The results labelled FE-Method 1 were derived using the thermal analysis models by omitting the thermal resistance of protection materials. Meanwhile, those labelled FE-Method 2 were obtained by considering the thermal resistance of the protection materials. As anticipated, the introduction of the thermal resistance of the protection material significantly decreased the temperature at the surface of the steel tube and concrete compared with the case without thermal resistance. The temperature deviation at the end of fire exposure was approximately 100 °C considering the partial of specimens as examples. This indicated the significant impact of the thermal resistance of the protection material on the temperature distribution. Furthermore, the thermal analysis model considering the thermal resistance of the protection material produced a smaller discrepancy in terms of temperature compared with the test results. This was employed in the following simulation to achieve an accurate analysis.

4.4 Mechanical model

A three-dimensional model was developed to simulate the mechanical behavior of SRCFST columns under the fire. The eight-node liner brick reduced integration element C3D8R was used for all the components. The concrete damage plasticity model in ABAQUS was used to simulate the mechanical properties of concrete. The stress–strain relationship at elevated temperature proposed by Han [44] was adopted here. It was modified based on the constitutive relationship at ambient

temperature. Note that the confinement effect of the steel tube was considered in the constitutive relationship. The stress–strain relationship at elevated temperature proposed by Lie [50] was adopted here to describe the mechanical behavior of steel. Surface-to-surface contact was used to model the interaction of between steel and concrete, with the steel tube and profiled steel, respectively, set as the master surfaces. To ensure an accurate input temperature from the heat transfer analysis to the mechanical analysis, the grid should be consistent between these. The initial geometrical imperfection of H / 1000 was adopted to consider this effect for the SRCFST columns with axial loading.

4.5 Validation of FE models

The developed FE models of protected SRCFST columns are validated in this subsection. The numerical results are compared with the obtained test data and observations. Graphical comparisons between the measured and predicted temperature evolution in time for the typical protected square SRCFST column specimens SSUP-Z-70-2 and SSUP-Z-80-3 are shown in Figs. 23–24. For the steel tube, the predicted temperature showed good agreement with the results measured at the measurement point 1 m below the mid-height of the column (T12), and was moderately lower for the measurement point at the mid-height of the column (T6). This was because the loss of fire protection during the fire exposure was omitted in the numerical models. For concrete and profiled steel, the temperature determined by FE calculation was also in good agreement with the test data.

In addition, validations were conducted for the axial deformation curves as well. The results are plotted in Fig. 25. The axial deformation curves obtained by numerical modeling are similar to the test results, although deviations in peak expansion and time attained peak expansion occurring. Finally, the critical data of all the eight SRCFST columns with fire protection for evaluating the fire resistance are listed in Table 6. The fire resistance and critical temperature of the steel tube at T12 determined by the numerical models and experimental results agree within a discrepancy less than 5%. This indicates that the results of FE calculation are likely to be of sufficient accuracy and reliability for the fire resistance.

5. Code comparison and current design predictions

5.1 General

Various design methods for fire resistance of CFST columns have been proposed by various countries and scholars. Most of these are aimed at CFST columns without fire protection. Branching from CFST columns, the study on fire design methods of SRCFST columns is just reports a few little. The methods for CFST columns are not applicable to SRCFST columns because of the improved fire resistance of SRCFST columns. Therefore, it is necessary to further evaluate the applicability of the above-mentioned design methods to SRCFST columns. For CFST columns with fire protection, the existing design rules regarding the thickness of fire protection as set out in GB 50936-2014, BS 5950-8:2003 and the design methods proposed by Han et al [44] are described in this subsection as a fire design guide for SRCFST columns. This would be assessed using the test data obtained in this study.

5.2 Chinese code (GB 50936-2014)

GB 50936-2014 provides a simple calculation equation that is specific for the protection thickness of CFST columns with non-intumescent fire protection materials. The thickness of fire resistive coating can be obtained by the following equation:

$$d = 16.4 \times \lambda (\frac{t_e}{t_{sc}} - 1) \qquad t < t_e \tag{4}$$

where d is the thickness of the protection (mm), λ is the thermal conductivity of the fire protective material (W/(m·°C)), t_{sc} is the fire resistance of the bare columns (min), and t_e is the fire resistance of the column with fire protection (min). Note that the fire resistance of the bare SRCFST columns were calculated using the FE models mentioned in Section 4 (see Table. 7). The measured data of the thermal conductivity of fire protective material in Section 2.3 (0.357 W/(m·°C)) was employed here.

5.3 British standard (BS 5950-8:2003)

According to BS 5950-8:2003, the thickness of fire protection required for a concrete-filled structural hollow section may be determined by multiplying the thickness of the fire protection required for a hollow structural section with an equal section factor (A_m / V) without concrete filling. The rate of increase in temperature of a steel member in a fire may be assumed to be proportional to

its section factor A_m / V (in m^{-1}) [43]. Here, A_m is the exposed surface area (in m) per unit length of member, and V is the volume of the member per unit length. In addition, the thickness required for a hollow section is determined from the thickness required for an I or H section with an equal section factor A_m / V (in m^{-1}) as follows:

$$\text{thickness} = t\{1 + (A_m / V) / 1000\} \qquad \text{for } A_m / V < 250 \tag{5a}$$

$$\text{thickness} = 1.25t \qquad \text{for } A_m / V > 250 \tag{5b}$$

The protection thickness of an I section is determined by the following equations:

$$d_p = \frac{A_m}{V} \lambda_p \frac{I_f}{10^6} F_w \quad \text{.....(6)}$$

where d_p is the protection thickness (m). F_w is the fire-protection material density factor and is determined as shown in *Eqs*. (7–8). It has a value between 0.6 and 1.0. λ_p is the thermal conductivity of the fire protective material (W/(m·°C)). I_f is the fire-protection material insulating factor (m^3/kW). It is obtained from the tabulation in BS 5950-8:2003.

$$F_w = \frac{(1+4\mu)^{0.5} - 1}{2\mu} \tag{7}$$

$$\mu = k_i \frac{\rho_p (1+0.03c)}{\rho_s} \frac{I_f}{10^6} \left(\frac{A_m}{V}\right)^2 \tag{8}$$

where k_i is a function of the thermal properties of insulation (W/(m·°C)) and is generally considered as 0.12 (W/(m·°C)) according to the manufacturer. ρ_p is the density of the protection material (kg/m^3), ρ_s is the density of steel, and c is the moisture content of the protection material (% by mass).

5.4 Calculation formula proposed by Han et al. [35]

Han *et al.* [44] provides a calculation method based on the results of parametric analyses supported by substantial experimental data. It is specified to the thick fire-resistive coating. Note that the effect of various load levels on protection thickness is considered in this method. The protection thickness under different load levels considering the influences of two types of section forms (circular, rectangular, and square sections) is given as follows:

For a circular section

$$a = k_{\mathrm{LR}}(19.2t + 9.6)C^{-(0.28-0.0019\lambda)} \tag{9a}$$

For rectangular and square sections

$$a = k_{\mathrm{LR}}(149.6t + 22)C^{-(0.42+0.0017\lambda - 2\times10^{-5}\lambda^2)} \tag{9b}$$

$$k_{\mathrm{LR}} = \begin{cases} pn + q & (k_{\mathrm{t}} \le n < 0.77) \\ 1/(3.695 - 3.5n) & (n \ge 0.77) \\ \omega(n - k_{\mathrm{t}})/(1 - k_{\mathrm{t}}) & \end{cases} \quad \begin{matrix} (k_{\mathrm{t}} < 0.77) \\ (k_{\mathrm{t}} \ge 0.77) \end{matrix} \tag{10}$$

where a is the thickness of the fire resistive coating, k_{LR} is a function of the load level n. k_{t} is the effect coefficient of bearing capacity under the fire, which can be obtained from [44] for simplicity. t is the fire resistance (h), C is the perimeter of the cross-section (mm), λ is the slenderness ratio (defined here as $4L / D$ for a circular section and $2\sqrt{3}\ L / B$ for a square section), $p = 1 / (0.77 - k_{\mathrm{t}})$, $q = k_{\mathrm{t}} / (k_{\mathrm{t}} - 0.77)$, and $\omega = 7.2t$ for a circular section and $10t$ for a square section. The properties of the thick fire-resistive coating adopted in Han's design equation are as follows: density $\rho = 400 \pm 20$ kg/m^3, thermal conductivity $\lambda_{\mathrm{p}} = 0.116$ (W/(m·°C)), and specific heat $c_{\mathrm{p}} = 1.047 \times 10^3$ J/(kg·k).

Note that the designed protection thickness needs to be recalculated according to *Eq.* 11 when the equivalent conductivity coefficient of the thick fire-resistive coating applied in the actual situation is not identified with that of the design requirement:

$$d_{\mathrm{i2}} = d_{\mathrm{i1}} \frac{\lambda_{\mathrm{i2}}}{\lambda_{\mathrm{i1}}} \tag{11}$$

where d_{i1} is the protection thickness specified in codes and documents (mm), d_{i2} is the protection thickness actually applied, λ_{i1} is the thermal conductivity of the fire protection materials specified in codes and documents (W/(m·°C)), and λ_{i2} is the thermal conductivity for fire protection materials actually applied (W/(m·°C)).

The design equation proposed by Han is limited to a load level in the fire scenario $n \leqslant 0.9$, fire resistance $t \leqslant 3$ h, slenderness ratio (λ) 10–80, concrete grade 30–90 MPa, steel grade 200–500 MPa, C = 800-8000 mm, and steel tube ratio (α_{st}) 0.03-0.20.

5.5 Evaluation of analytical predictions of protection thickness

In this subsection, the design methods described above are compared with the fire test performed in this study. The quantitative assessments of design protection thickness through comparisons with the design thickness and the corresponding actually applied thickness are reported in Table 7 and Fig. 26 respectively. The accuracy of design thickness is evaluated in terms of the ratio between the design protection thickness and actually applied thickness in the test. The graphical and quantitative assessments reveal that (i) overall, the three design methods overestimate the protection thickness of SRFCST column under fire; (ii) the method in BS 5950-8:2003 provides the most conservative design method; (iii) Han's equations predict the protection thickness more accurately, although with an overestimation of 59.7%; (iv) and GB 50936-2014 yields the most scattered protection thickness prediction overall.

The influence of load level on accuracy of design protection thickness is presented in Fig. 27. BS 5950-8:2003 provides safe predictions for all SRCFST columns to achieve fire protection, because the empirical formula in BS 5950-8:2003 is only based on the one-dimensional passage of heat through a thin fire protective material into a steel section. GB 50936-2014 overestimates the protection thickness of SRCFST columns, except for SRCFST columns with load level of 0.6. The load level and eccentricity have been accounted in parametric analysis conducted by Han, and the effect of eccentricity on fire resistance has been neglected in design equation. Thus, Han's method provides unsafe predictions for specimens CSUP-P50-50-1 (n=0.5) and SSUP-Z-60-1 (n=0.6), which shows low protection thickness with an underestimation of approximately 25%. However, for SRCFST columns with load level lower than 0.6(specimens CSUP-P50-50-1 and SSUP-Z-60-1), the design method in Han provides the closer predictions, compared with those of SRCFST columns with load level larger than effective load of 0.77.

Finally, the present design method cannot be applied to safely and accurately predict the fire protection thickness of SRCFST columns (specific to thick fire-resistive coating). Although the design method proposed by Han considers various parameters including geometric, material, and load parameters, the design method needs to be corrected or reproposed in a further study.

6. Conclusion

In this study, experimental investigations and numerical modeling were conducted to study the fire behavior and resistance of SRCFST columns with thick fire-resistive coating under the ISO-834 standard fire. The followings are the conclusions:

(1) All the specimens with fire resistive coating presented global failure and were destroyed abruptly. No local buckling could be observed in the flange of the profiled steel although the protected SRCFST specimens sustained a higher load level in the present test. This was unlike the SRCFST columns without fire protection. A plateau can be observed at approximately 200 °C in the temperature curves of the steel tube. This was caused by the evaporation of free water in the fire resistive coating. The temperature of profiled steel remained below 250 °C at the end of fire exposure. This reveals that the presence of profiled steel significantly improved the fire performance of SRCFST columns with fire resistive coating.

(2) The fire resistance of SRCFST columns can be improved significantly by applying fire protection. SRCFST columns with a high load level (n > 0.6) had fire resistance higher than 1 h because of the application of a thick fire-resistive coating. The fire resistance of the SRCFST specimen with a protection thickness of 12 mm was 3.32 times that of bare specimens under an identical load level. In addition, the improvement in the fire resistance of the SRCFST columns under eccentric compression tended to be faster than that for the SRCFST columns under axial compression when applied with fire protection of an equal thickness.

(3) The thermal properties recommended in EC4 yield more accurate and consistent temperature predictions. The thermal resistance of the protection material should be considered in a thermal analysis model to produce a smaller discrepancy in terms of temperature compared with the test results.

(4) The obtained test results and predicted data were used to estimate the accuracy and applicability of fire protection thickness in present design methods. GB 50936-2014 overestimated the protection thickness of SRCFST columns and caused the most scattered protection thickness

prediction due to regardless of their load level and eccentricity. The method in BS 5950-8:2003 provides the most conservative design method. However, it has the maximum error on an average. The regression formula proposed by Han et al. is the closest design method. However, it may be unsafe for SRCFST columns with a load level lower than 0.6.

Acknowledgements

The research reported in this study is a project supported by National Natural Science Foundation of China (Nos. 51778274 & 52168020). The authors wish to express their sincere gratitude for this support.

References

[1] EN 1994-1-1. Design of composite steel and concrete structures, Part 1.1, general rules and rules for buildings. European Committee for Standardization: Brussels, Belgium; 2004.

[2] Wang QX, Zhao DZ, Guan P. Experimental study on the strength and ductility of steel tubular columns filled with steel-reinforced concrete. Eng Struct 2004; 26:907-915.

[3] Chang X, Wei YY, Yun YC. Analysis of steel-reinforced concrete-filled steel tubular (SRCFST) columns under cyclic loading. Constr Build Mater 2012; 28: 88-95.

[4] Xian W, Chen WS, Hao H, Wang WD. Experimental and numerical studies on square steel-reinforced concrete-filled steel tubular (SRCFST) members subjected to lateral impact. Thin-Walled Struct 2021; 160: 107409 (1-18).

[5] Farajpourbonab E, Kute SY, Inamdar VM. Steel-reinforced concrete-filled steel tubular columns under axial and lateral cyclic loading. Int J Advan Struct Eng 2018; 10: 61-72.

[6] Ding FX, Zhang T, Liu XM, Guo Q, Jiang GS. Behavior of steel-reinforced concrete-filled square steel tubular stub columns under axial loading. Thin-Walled Struct 2017; 119: 737-748.

[7] Wang WD, Jia ZL, Shi YL, Tan EL. Performance of steel-reinforced circular concrete-filled steel tubular members under combined compression and torsion. J Constr Steel Res 2020; 173: 106271(1-16).

[8] Wang JH, He J, Xiao Y. Fire behavior and performance of concrete-filled steel tubular columns:

Review and discussion. J Constr Steel Res 2019; 157: 19-31.

[9] Zhou XH, Yan B, Liu JP. Behavior of square tubed steel reinforced-concrete (SRC) columns under eccentric compression. Thin-Walled Struct 2015; 91: 129-138.

[10] Xie WT, Chen Y, Han SH, Zhou WB, He K. Research on I steel reinforced concrete-filled GFRP tubular short columns. Thin-Walled Struct 2017; 120: 282-296.

[11] Wang JH, He J, Xiao Y. Fire behavior and performance of concrete-filled steel tubular columns: Review and discussion. J Constr Steel Res 2019; 157: 19-31.

[12] Han LH, Chen F, Liao FY, Tao Z, Uy B. Fire performance of concrete filled stainless steel tubular columns. Eng Struct 2013; 56: 165-181.

[13] Lie TT, Chabot M. Experimental studies on the fire resistance of hollow steel columns filled with plain concrete. NRC-CNRC Internal Report, 1992, No.611.

[14] Tretyakov A, Tretyakov I, Wald F. Fire response model of the steel fibre reinforced concrete filled tubular column. J Constr Steel Res 2021; 186: 106884.

[15] Moradi MJ, Daneshvar K, Ghazi-nader D, Hajiloo H. The prediction of fire performance of concrete-filled steel tubes (CFST) using artificial neural network. Thin-Walled Struct 2021; 161: 107499.

[16] Yao Y, Li H, Guo HC, Tan KH. Fire resistance of eccentrically loaded slender concrete-filled steel tubular columns. Thin-Walled Struct 2016; 106: 102-112.

[17] Wang K, Young B. Fire resistance of concrete-filled high strength steel tubular columns. Thin-Walled Struct 2013; 71: 46-56.

[18] Ibañez C, Romero ML, Hospitaler A. Fiber beam model for fire response simulation of axially loaded concrete filled tubular columns. Eng Struct 2013; 56: 182-193.

[19] Pires TAC, Rodrigues JPC, Silva JJR. Fire resistance of concrete filled circular hollow columns with restrained thermal elongation. J Constr Steel Res 2012; 77: 82-94.

[20] Moradi MJ, Daneshvar K, Ghazi-nader D, Hajiloo H. The prediction of fire performance of concrete-filled steel tubes(CFST) using artificial neural network. Thin-Walled Struct 2021; 161:

107499.

[21] Kamil GM, Liang QQ, Hadi MNS. Fiber element simulation of interaction behavior of local and global buckling in axially loaded rectangular concrete-filled steel tubular slender columns under fire exposure. Thin-Walled Struct 2019; 145: 106403.

[22] Kamil GM, Liang QQ, Hadi MNS. Fire-resistance of eccentrically loaded rectangular concrete-filled steel tubular slender columns incorporating interaction of local and global buckling. Int J Struct Stab Dy 2019; 19(8): 1950085.

[23] Chu TB, Gernay T, Dotreppe JC, Franssen JM. Steel hollow columns with an internal profiled filled with self-compacting concrete under fire conditions. Proceedings of the Romanian Academy Series a-Mathematics Physics Technical Sciences Information Science 2016; 17(2): 152-159.

[24] Tan QH, Gardner L, Han LH, Song TY. Fire performance of steel reinforced concrete-filled stainless steel tubular columns with square cross-sections. Thin-Walled Struct 2019; 143: 106197.

[25] Espinos A, Romero ML, Lam D. Fire performance of innovative steel-concrete composite columns using high strength steels. Thin-Walled Struct 2016; 106: 113-128.

[26] Schaumann P, Kleibomer I. Experimental and numerical investigations of the composite behaviour in concrete-filled tubular columns with massive steel core at high temperatures. Struct in Fire 2016: 544-551.

[27] Neuenschwander M, Knobloch M, Fontana M. Modeling thermo-mechanical behavior of concrete-filled steel tube columns with solid steel core subjected to fire. Eng Struct 2017; 136: 180-193.

[28] Neuenschwander M, Knobloch M, Fontana M. ISO standard fire tests of concrete-filled steel tube columns with solid steel core. J Struct Eng 2017; 143(4): 04016211.

[29] Neuenschwander M, Knobloch M, Fontana M. Fire tests of concrete-filled circular hollow section columns with solid steel core. Composite Construction in Steel and Concrete VII 2016;

508-521.

[30] Meng FQ, Zhu MC, Mou B, He BJ. Residual strength of steel-reinforced concrete-filled square steel tubular (SRCFST) stub columns after exposure to ISO-834 standard fire. Int J Steel Struct 2019; 19(3): 850-866.

[31] Yang X, Tang C, Chen Y, Qiao TY. Compressive behavior of steel-reinforced concrete-filled square steel tubular stub columns after exposure to elevated temperature. Eng Struct 2020; 204: 110048.

[32] Lucherini A, Maluk C. Intumescent coatings used for the fire-safe design of steel structures: A review. J Constr Steel Res 2019; 162: 105712.

[33] Häßler D, Hothan S. Performance of intumescent fire protection coatings applied to structural steel tension members with circular solid and hollow sections. Fire Saf J 2022; 131: 103605.

[34] Cirpici BK, Wang YC, Rogers B. Assessment of the thermal conductivity of intumescent coatings in fire. Fire Saf J 2016; 81: 74-87.

[35] Correia JR, Branco FA, Ferreira JG, Bai Y, Keller T. Fire protection systems for building floors made of pultruded GFRP profiles-Part 1: Experimental investigations. Compos: Part B 2010; 41: 617-629.

[36] Bai Y, Keller T, Correia JR, Branco FA, Ferreira JG. Fire protection systems for building floors made of pultruded GFRP profiles-Part 2: Modeling of thermomechanical responses. Compos: Part B 2010; 41: 630-636.

[37] Liu K, Chen W, Ye JH, Bai Y, Jiang J, Tong YK, Chen WW. Improved fire resistance of cold-formed steel walls by using super absorbent polymers. Thin-Walled Struct 2021; 160: 107355.

[38] Chen W, Liu K, Ye JH, Jiang J. Fire performance of superabsorbent polymers protecting cold-formed steel walls with high load ratios. Thin-Walled Struct 2022; 181: 110092.

[39] Han LH, Xu L, Zhao XL. Tests and analysis on the temperature field within concrete filled strrl tubes with or without protection subjected to a standard fire. Advan in Struct Eng 2003; 6: 121-133.

[40] Yu M, Hu X, Chi Y, Ye JQ. A unified method for calculating the fire resistance of concrete-filled steel tube with fire protection under combined loading. J Constr Steel Res 2020; 168: 106003.

[41] Yin L, Ni ZP, Ye JH, Qiu PF. Study on fire protection performance of CFST mega-columns protected by thick coated fire resistive coatings. J Build Struct 2015; 36(s1): 305-309.

[42] GB 50936-2014. Technical code for concrete filled steel tubular structures. China Architecture &Building Press: Beijing, China; 2014.

[43] BS 5950-8:2003. Structural Use of Steelwork in Buildings, Part 8: Code of Practice for Fire Resistance Design[S]. British Standards Institution, 1990.

[44] Han LH. Concrete Filled Steel Tubular Structures-Theory and Practice, 3rd ed. Science press: Beijing, China; 2016.

[45] Mao WJ, Wang WD, Zhou K, Du EF. Experimental study on steel-reinforced concrete-filled steel tubular columns under the fire. J Constr Steel Res 2021; 185: 106867.

[46] DG/TJ 08-008-2017. Technical code on fire safety of steel building structures. Tongji University Press: Shanghai, China; 2017.

[47] GB 14907-2018. Fire resistive coating for steel structure. Chinese Standard Press: Beijing, China; 2018.

[48] ISO 834-1: 1999. Fire-resistance tests-elements of building construction-Part 1: General requirements. International organization for standardization, Geneva; 1999.

[49] EN 1993-1-2. Design of steel structures-Part 1.2: General rules-Structural fire design. European Committee for Standardization: Brussels, Belgium; 2005.

[50] Lie TT. Fire resistance of circular steel columns filled with bar-reinforced concrete. J Struct Eng 1994; 120(5): 1489-1509.

[51] EN 1994-1-2. Design of composite steel and concrete structures-Part 1-2: General rules-Structural fire design: Brussels, Belgium; 2005.

Nomenclature

t	wall thickness of steel tube or fire during time
H	length of composite column
n	load ratio, $n = N_F / N_u$
λ_i	equivalent conductivity coefficient
c	percentage moisture content in the material
d	thickness of fire resistive coating or steel plate
t_v	delay time
λ_p	thermal conductivity of fire protective material
ρ_p	densities of insulation
N_F	constant load applied on the column in the test
N_u	ultimate bearing capacity of the column at ambient temperature
e	Eccentricity
f_y	yield strength of steel
f_u	ultimate strength of steel
E_s	modulus of elasticity of steel
μ_s	Poisson' ratio of steel
δ_{10}(%)	elongation
A_m	exposed surface area (in m) per unit length of member
V	volume of member per unit length
T_{cr}	critical temperature
t_R	fire resistance
t_{sc}	fire resistance of bare columns
$t_{R.test}$	tested fire resistance
d_{test}	measured thickness of fire resistive coating
d_{GB}	thickness of fire resistive coating predicted using the calculation method in GB 50936-2014

d_{Han} thickness of fire resistive coating predicted using the regression formula by Han *et al.*

$d_{BS\ 5950}$ thickness of fire resistive coating predicted using the calculation equation in BS 5950-2003

Tables

Table 1 Measured geometric dimensions of SRCFST specimens

Specimen ID	Profile steel	Steel tube ratio, α_{st}	Profile steel ratio, α_{ss}	Load eccentricity (mm)	thickness of fire protection, d (mm)	Load level, n	Applied load(kN)	Fire Resistance time, t_R (min)
CSUP-P50-50-1	*A*	0.068	0.046	50	12	0.5	1767	103
CSUP-P50-70-2	*A*	0.068	0.046	50	14	0.7	2474	83
CSUP-P80-70-3	*A*	0.068	0.046	80	14	0.7	2019	63
CSUP-P80-70-4	*A*	0.068	0.046	80	12	0.7	2019	57
SSUP-Z-60-1	*B*	0.082	0.056	0	17	0.6	3667	102
SSUP-Z-70-2	*B*	0.082	0.056	0	12	0.7	4274	78
SSUP-Z-80-3	*B*	0.082	0.056	0	12	0.8	4885	62
SSUP-Z-80-4	*B*	0.082	0.056	0	17	0.8	4885	83

*Steel tube ratio, α_{st}, is defined as the ratio of cross-sectional area of steel tube to concrete, and profiled steel ratio, α_{ss}, is the ratio of cross-sectional area of profiled steel and concrete. Load level, n, is defined as the ratio of applied load during the fire test and the buckling resistance of SRCFST column specimens at ambient according to EN 1994-1-1.

Table 2 Material properties of steel

Cross-section	Grade	E_s(GPa)	f_y(MPa)	f_u(MPa)	μ_s	δ_{10}(%)	f_y/f_u
Circular steel tube	235	193.04	345.02	455.17	0.29	35	0.76
squarer steel tube	235	181.44	325.55	458.58	0.29	41	0.71
Steel plane-5mm	235	174.49	276.59	419.74	0.29	37	0.66
Steel plane -8mm	235	154.63	260.79	412.37	0.29	40	0.63

Table 3 Mixture proportions of concrete (relative to weight of cement)

Concrete grade	Cement	Water	Sand	Gravel	Pulverized coal ash	Mineral powder	Polycarboxylate-type superplasticizer
C50	1.00	0.35	1.69	2.38	0.15	0.09	0.017
C70	1.00	0.47	1.48	2.42	0.36	0.11	0.022

Table 4 Summaries of fire resistance time for unprotected and protected SRCFST columns

Specimen ID	n	e (mm)	d/mm	t_R/ t_R* (min)	t_R/ t_R*	Specimen ID	n	e (mm)	d/mm	t_R/ t_R* (min)	t_R/ t_R*
CSU-P50-40*	0.40	50	0	31	1.00	SSU-Z-40*	0.39	0	0	74	1.00
CSUP-P50-50-1	0.50	50	12	103	3.32	SSU-Z-50	0.49	0	0	48	0.65
CSUP-P50-70-2	0.70	50	14	83	2.68	SSUP-Z-60-1	0.60	0	17	102	1.38
CSU-P80-40*	0.46	80	0	19	1.00	SSUP-Z-70-2	0.70	0	12	78	1.05
CSUP-P80-70-3	0.70	80	14	63	3.32	SSUP-Z-80-3	0.80	0	12	62	0.84
CSUP-P80-70-4	0.70	80	12	57	3.00	SSUP-Z-80-4	0.80	0	17	83	1.12

Table 5 Comparison of measured and predicted temperature of bare SRCFST column specimens

Steel tube									
Specimen ID	$T_{cr.T6}$	$T_{cr.T12}$	$T_{cr.Avg}$	T.T Lie		EN 1994-1-2		BS 5950	
				$T_{cr.Lie}$	$T_{cr.Lie}/T_{cr.Avg}$	$T_{cr.EC4}$	$T_{cr.EC4}/T_{cr.Avg}$	$T_{cr.BS\ 5950}$	$T_{cr.BS\ 5950}/T_{cr.Avg}$
CSU-Z-40	648	—	648	815	1.257	813	1.254	814	1.263
CSU-Z-50	502	492	497	447	0.899	446	0.897	443	1.114
CSU-P50-40	530	496	513	555	1.082	545	1.062	546	1.073
CSU-P80-40	408	433	420	412	0.980	398	0.947	406	0.826
SSU-Z-40	665	671	668	834	1.249	848	1.269	844	1.255
SSU-Z-50	671	683	677	746	1.102	731	1.081	754	0.891
SSU-P50-40	553	548	550	592	1.076	574	1.043	591	1.065
SSU-P80-40	395	395	395	327	0.827	331	0.838	326	0.965
				Mean	1.059		1.049		1.057
				Std.dev	0.153		0.156		0.158
Concrete									
Specimen ID	$T_{cr.T5}$	$T_{cr.T10}$	$T_{cr.Avg}$	T.T Lie		EN 1994-1-2		BS 5950	
				$T_{cr.Lie}$	$T_{cr.Lie}/T_{cr.Avg}$	$T_{cr.EC4}$	$T_{cr.EC4}/T_{cr.Avg}$	$T_{cr\ BS\ 5950}$	$T_{cr.BS\ 5950}/T_{cr.Avg}$
CSU-Z-40	111	—	111	101	0.912	122	1.100	138	1.243
CSU-Z-50	43	46	45	30	0.664	40	0.893	40	0.905
CSU-P50-40	63	73	68	44	0.642	63	0.920	62	0.909
CSU-P80-40	50	32	41	27	0.653	33	0.820	35	0.850
SSU-Z-40	148	—	148	133	0.900	157	1.060	130	0.879
SSU-Z-50	110	—	110	122	1.108	144	1.310	121	1.098
SSU-P50-40	89	—	89	23	0.253	27	0.303	24	0.275
SSU-P80-40	33	32	33	51	1.567	69	2.120	58	1.782
				Mean	0.837		1.066		0.993
				Std.dev	0.389		0.520		0.424
Mean					0.948		1.025		1.057
Std.dev					0.289		0.293		0.346

Table 6 Comparison of FE results and test results

Specimen ID	$T_{cr.test-T6}$ (℃)	$T_{cr.test-T12}$ (℃)	$t_{R.Test}$ (min)	$T_{cr.FE}$ (℃)	$t_{R.FE}$ (min)	$T_{cr.FE}/T_{cr.test-T6}$	$T_{cr.FE}/T_{cr.test-T12}$	$t_{R.FE}/t_{R.test}$
CSUP-P50-50-1	525.2	524.6	103	433.8	98	0.828	0.827	0.951
CSUP-P50-70-2	471.8	383.8	83	394.5	69	1.028	0.836	0.831
CSUP-P80-70-3	434.7	355.0	63	335.5	62	0.945	0.772	0.984
CSUP-P80-70-4	418.8	352.7	57	319.3	51	0.905	0.762	0.895
SSUP-Z-60-1	458.2	372.9	102	393.8	111	0.859	1.056	1.088
SSUP-Z-70-2	501.9	410.6	78	472.9	79	0.942	1.152	1.013
SSUP-Z-80-3	566	428.1	62	422.3	56	0.986	0.746	0.903
SSUP-Z-80-4	364.2	——	83	375.5	86	1.031	——	1.036
Mean						0.869	0.961	0.963
COV						0.113	0.139	0.087

Table 7 Summary of protection thickness for SRCFST columns according to three methods

Specimen ID	$t_{R.test}$ (min)	t_{sc} (min)	d_{test} (mm)	GB 50936-2014		BS 5950-8:2003		Han *et al.*	
				d_{GB} (mm)	d_{GB}/d_{test}	$d_{BS\ 5950}$(mm)	$d_{BS\ 5950}/d_{test}$	d_{Han}(mm)	d_{Han}/d_{test}
CSUP-P50-50-1	103	28	12	15.683	1.307	51.724	4.310	9.050	0.754
CSUP-P50-70-2	83	8.3	14	52.693	3.764	48.575	3.470	25.698	1.836
CSUP-P80-70-3	63	8	14	40.252	2.875	41.743	2.982	21.150	1.511
CSUP-P80-70-4	57	8	12	35.861	2.988	40.014	3.335	19.785	1.649
SSUP-Z-60-1	102	27	17	16.263	0.957	60.971	3.587	13.150	0.774
SSUP-Z-70-2	78	20	12	16.979	1.415	42.236	3.520	22.834	1.903
SSUP-Z-80-3	62	15	12	18.345	1.529	28.506	2.376	27.058	2.255
SSUP-Z-80-4	83	15	17	26.542	1.561	61.061	3.592	33.234	1.955
Mean					2.049		3.396		1.579
COV					0.462		0.153		0.325

Figures

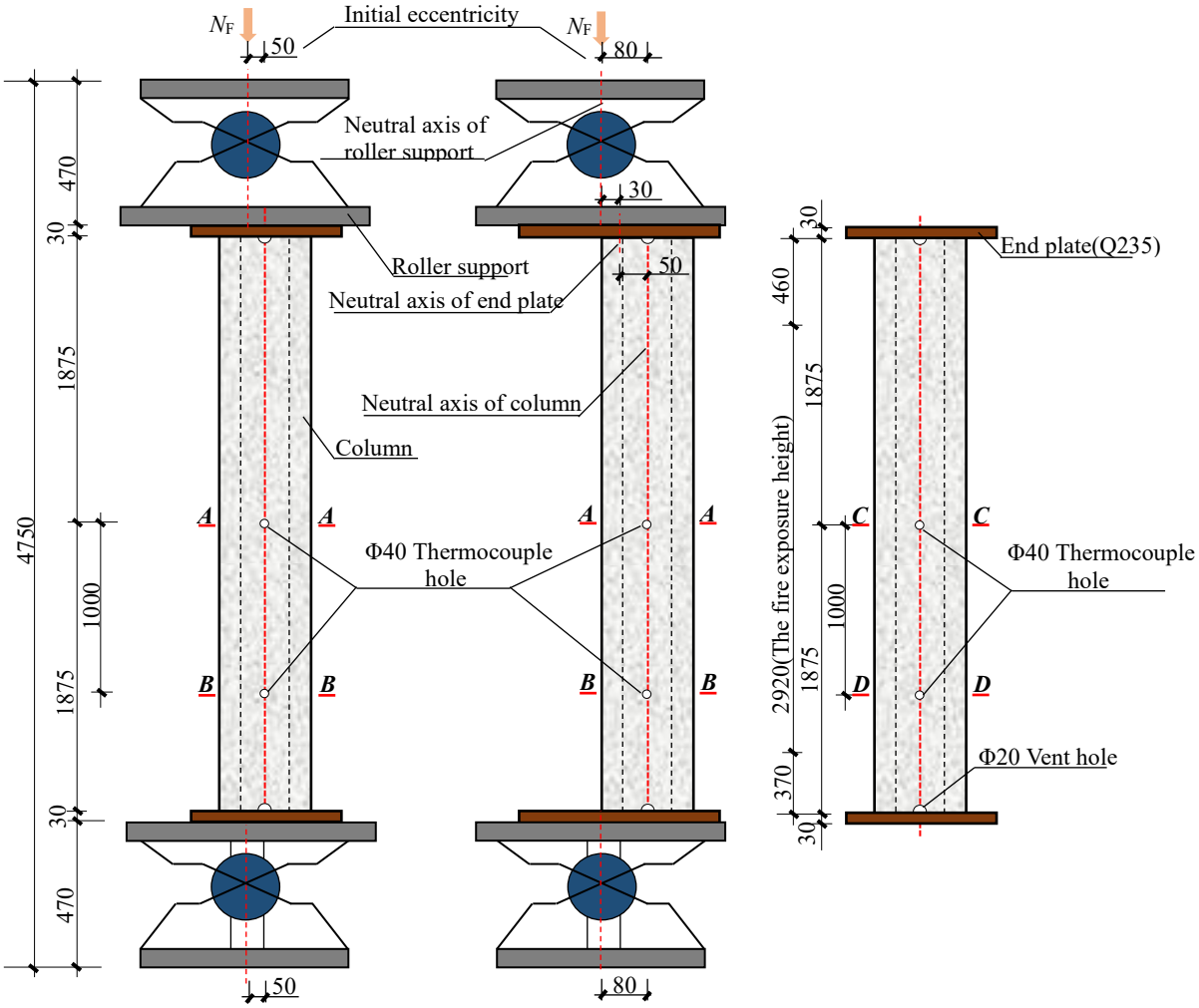

Fig.1 Longitudinal dimensions of specimens (unit: mm) (a) Column with eccentricity of 50(CSUP-P50-50-1, CSUP-P50-70-2); (b) Column with eccentricity of 80(CSUP-P80-70-3, CSUP-P80-70-4) (c) Column with axial loading (SSUP-Z-60-1, SSUP-Z-70-2, SSUP-Z-80-3, SSUP-Z-80-4)

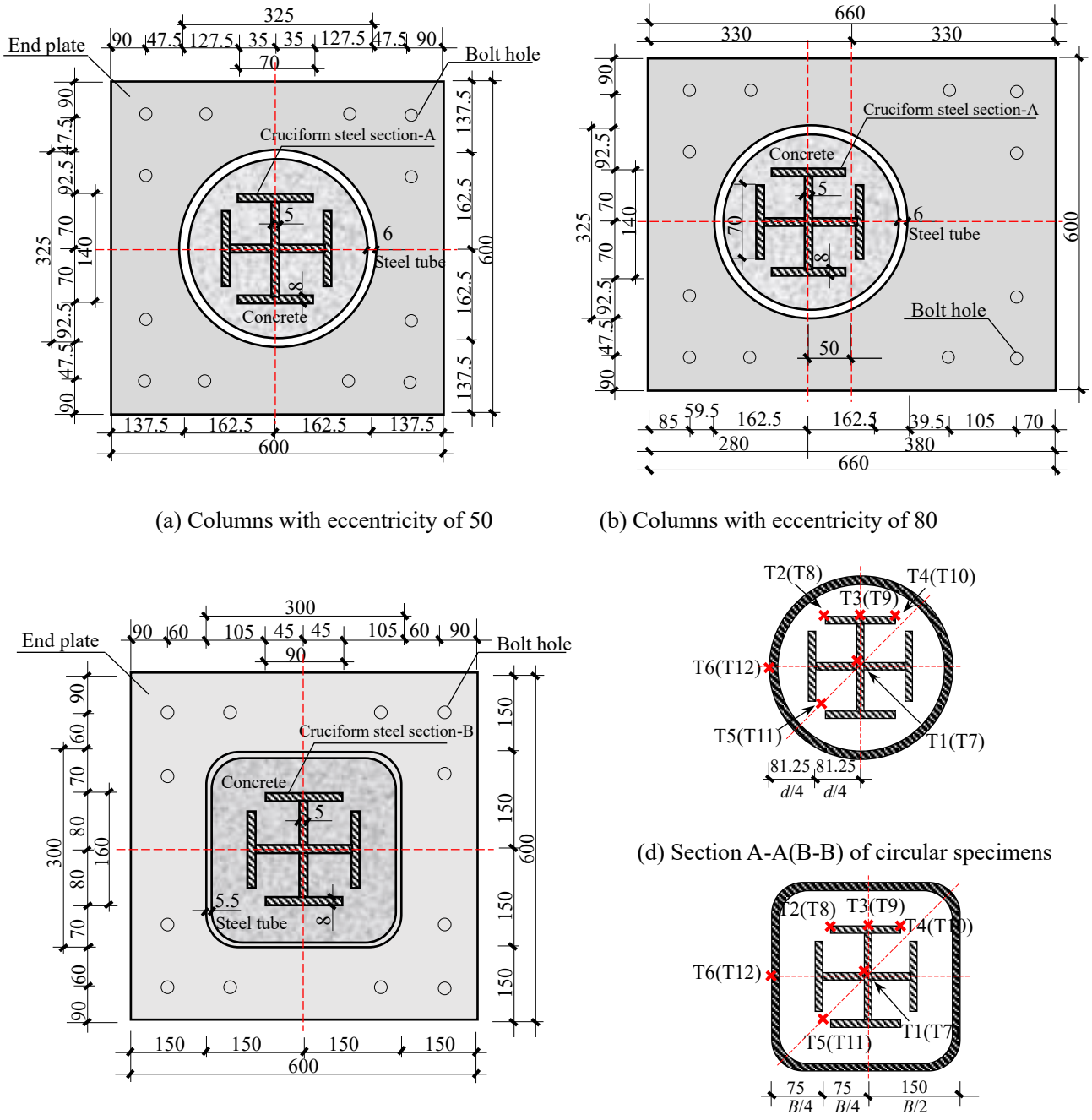

(a) Columns with eccentricity of 50

(b) Columns with eccentricity of 80

(c) Columns with axial loading

(d) Section A-A(B-B) of circular specimens

(e) Section C-C(D-D) of square specimens

Fig.2 Cross-sectional dimensions and locations of thermocouples in the cross-section (unit: mm)

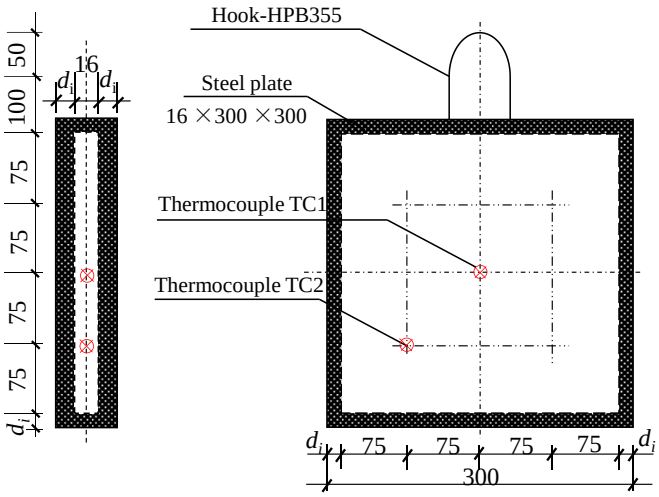

Fig.3 Details of test coupons and positions of thermocouples (unit: mm)

Fig.4 Fire furnace

(a) Before fire test (b) After fire test

Fig.5 Surface conditions of test coupons before fire test and after fire test

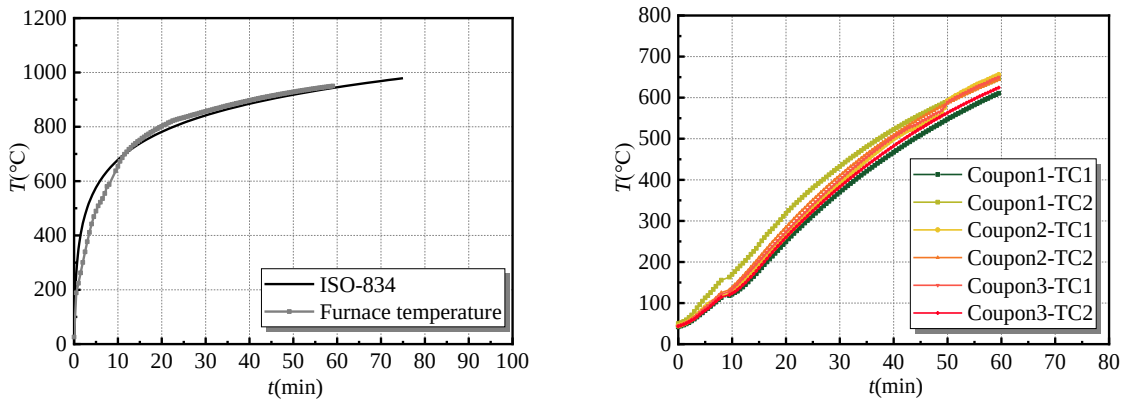

(a) Comparisons of furnace temperature and ISO-834 curve (b) Temperature in test coupons during fire test

Fig.6 Measured temperature (T) versus time (t) relationships

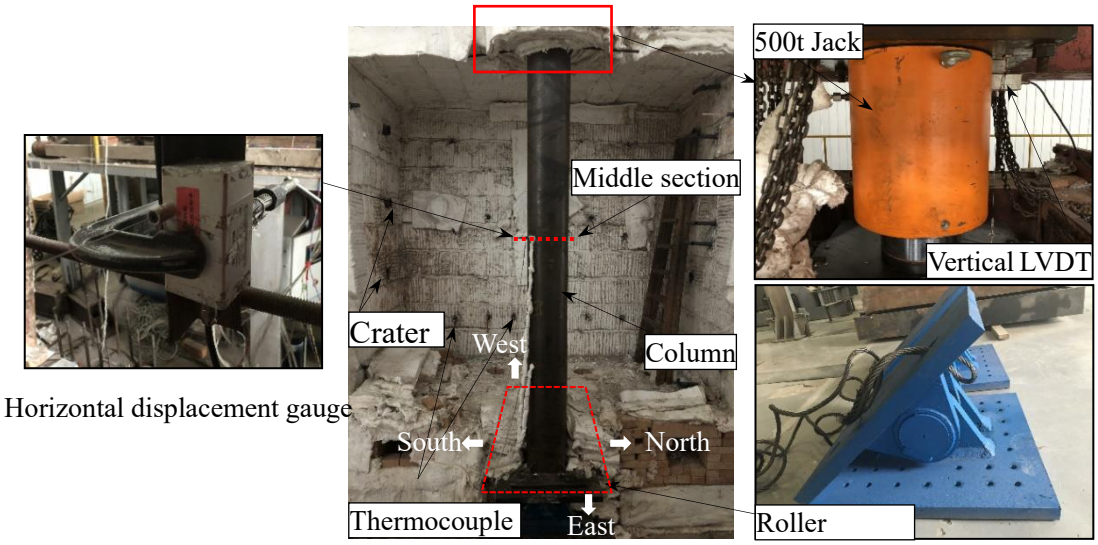

Fig.7 Details of test setup and position of SRCFST column specimen in fire furnace

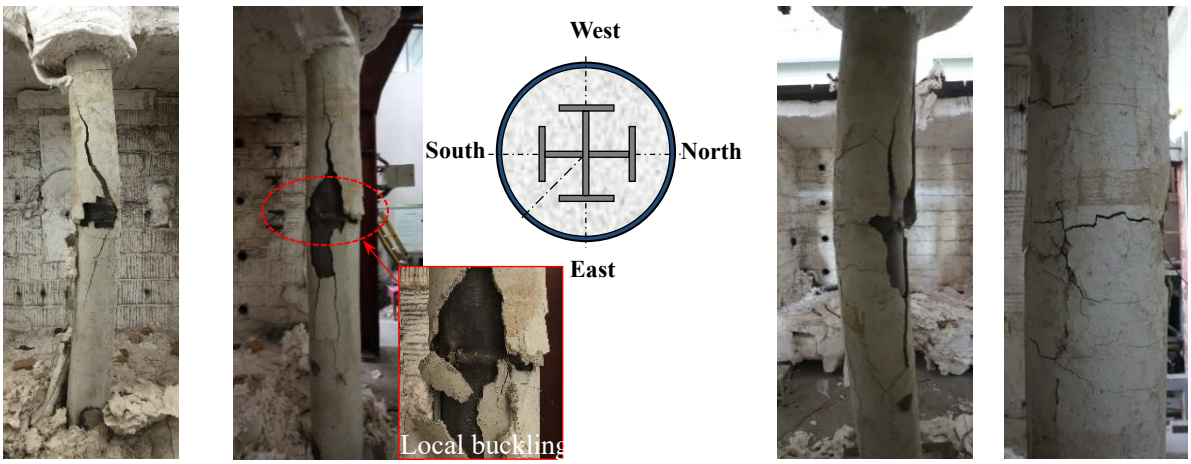

(a) East (b) South (c) Position of columns inside the furnace (d) West (e) North

Fig.8 The failure mode of CSUP-P50-50-1 after the fire exposure

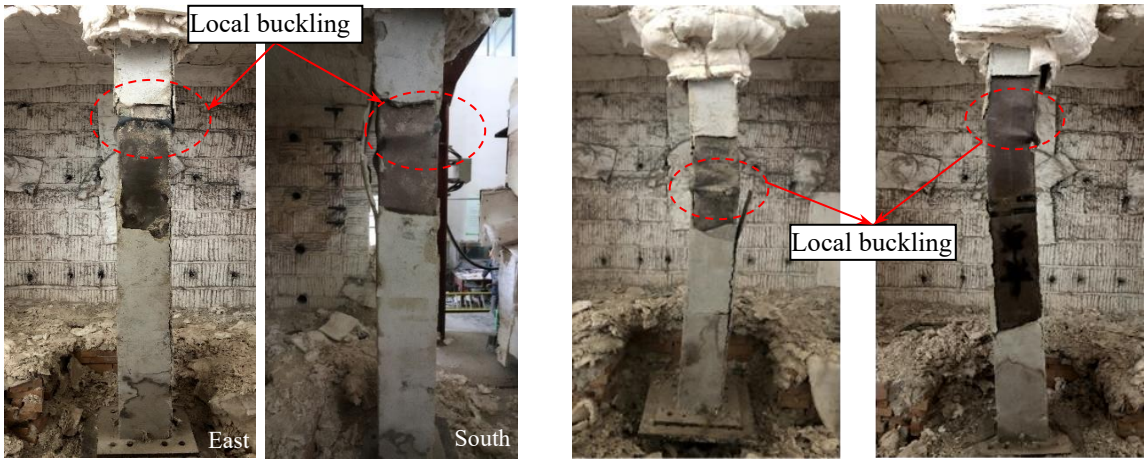

(a) SSUP-Z-60-1 (b) SSUP-Z-80-3 (c) SSUP-Z-80-4

Fig.9 The failure mode of typical square SRCFST specimens after the fire exposure

Fig.10 Comparison of failure modes for SRCST column specimens after removing the fire resistive coating (West)

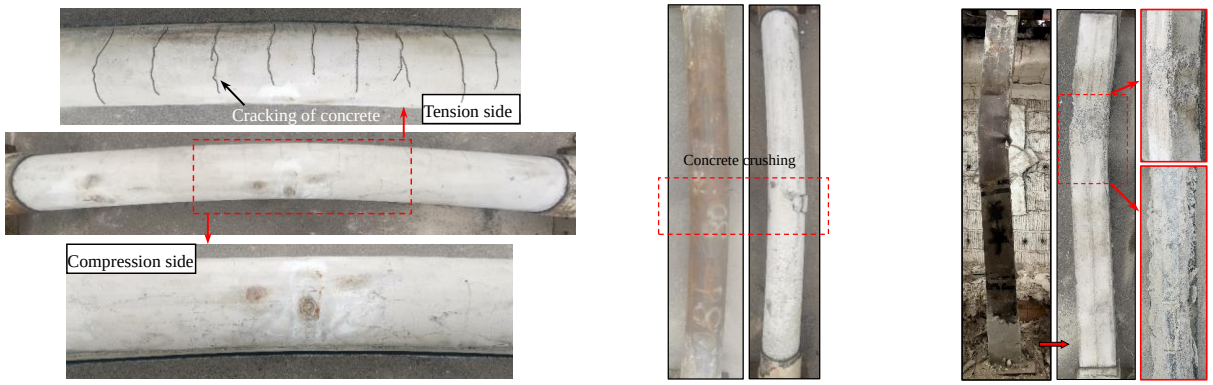

(a) Concrete modes of CSUP-P80-70-3 (b) Concrete modes of CSUP-P80-70-4 (c) Inner states of SSUP-Z-80-4

Fig.11 Inner failure modes of the SRCFST specimens after the fire exposure

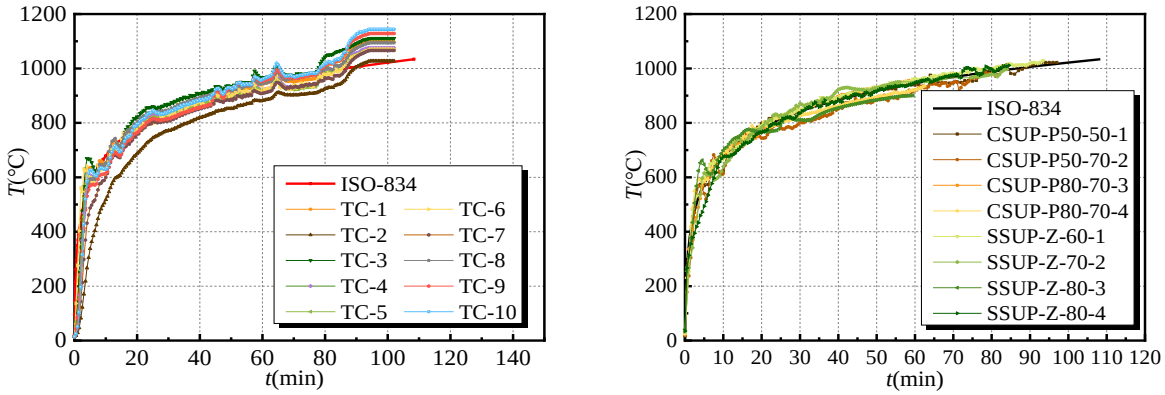

(a) Measured furnace temperature of CSUP-P50-50-1 (b) Average furnace temperature of SRCFST specimens

Fig.12 Comparison between tested furnace temperature curves and ISO-835 standard curve

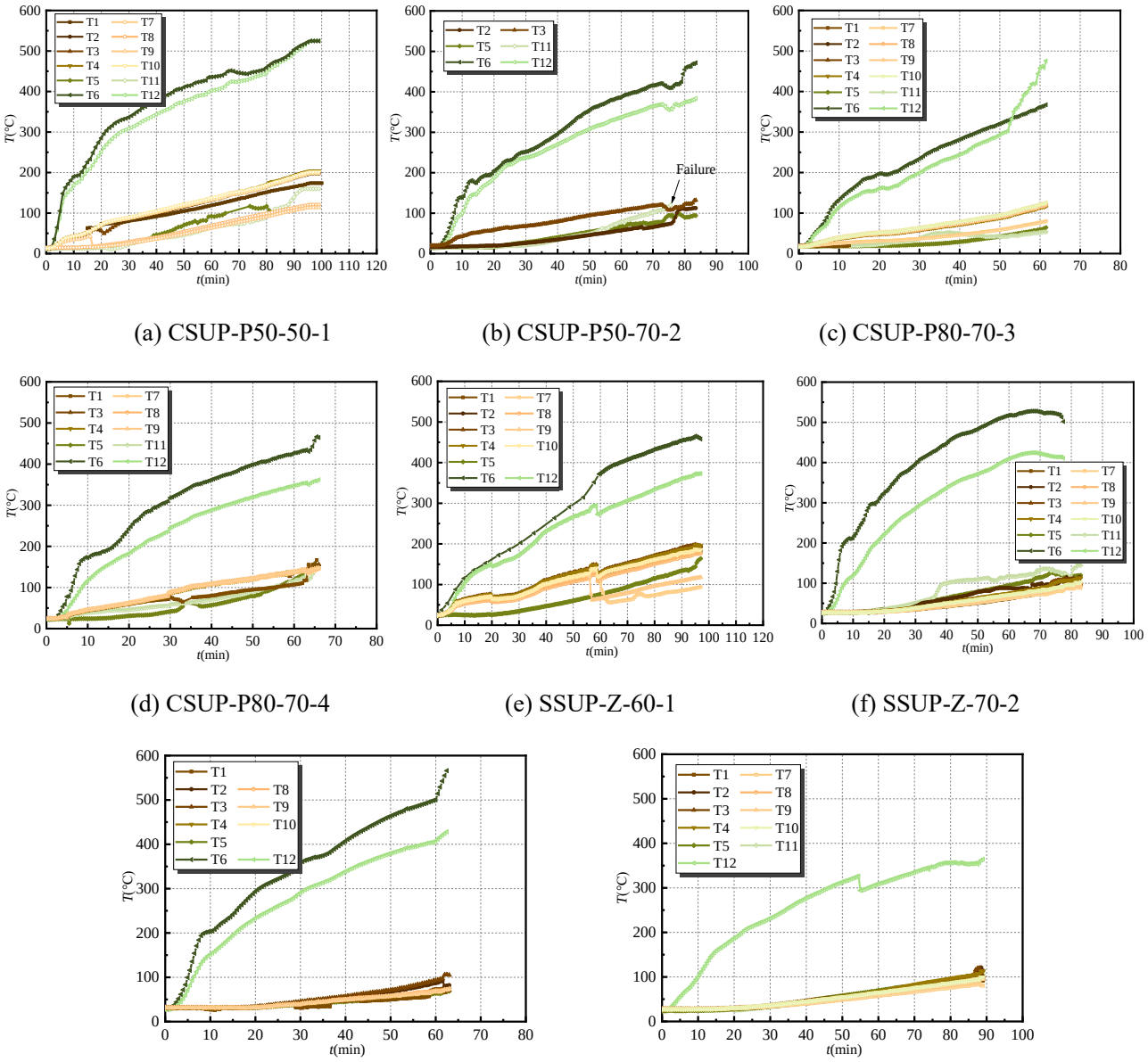

(a) CSUP-P50-50-1 (b) CSUP-P50-70-2 (c) CSUP-P80-70-3

(d) CSUP-P80-70-4 (e) SSUP-Z-60-1 (f) SSUP-Z-70-2

(g) SSUP-Z-80-3 (h) SSUP-Z-80-4

Fig.13 Measurement of temperature during the fire test of SRCFST column specimens

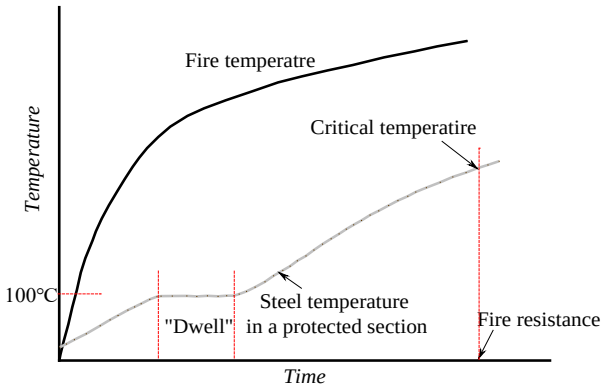

Fig.14 Typical heating curve for a protected steel section

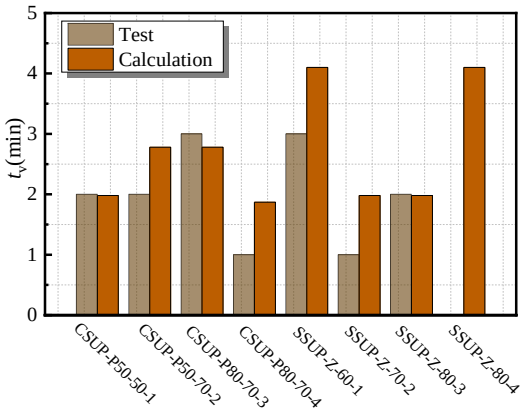

Fig.15 Comparison of delay time tv between tested and calculated data

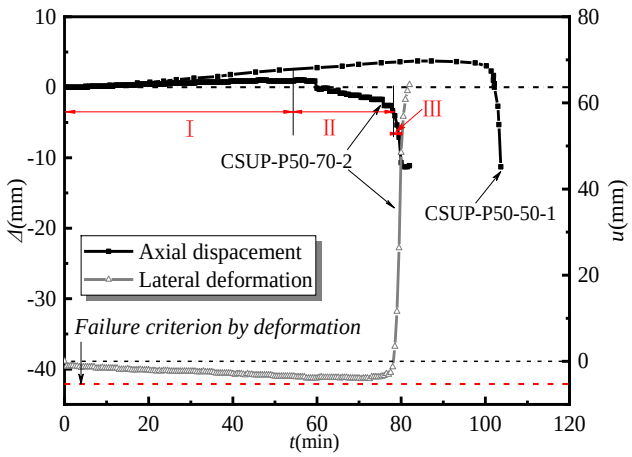

(a) SRCFST specimens with eccentricity of 50mm

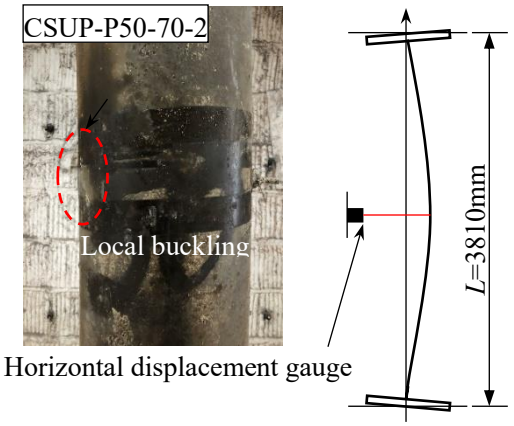

(b) Local buckling and remaining bending line

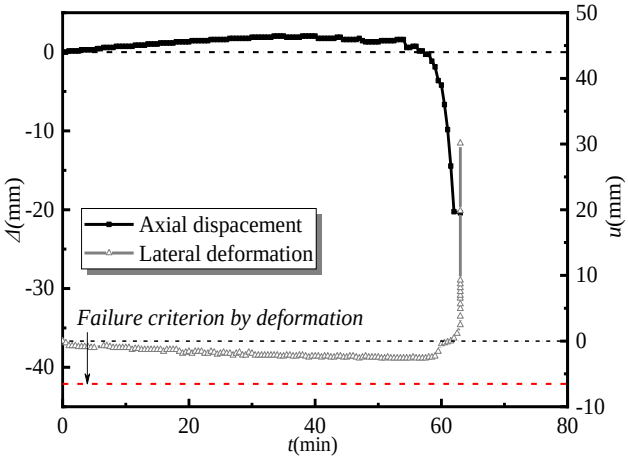

(c) CSUP-P80-70-3

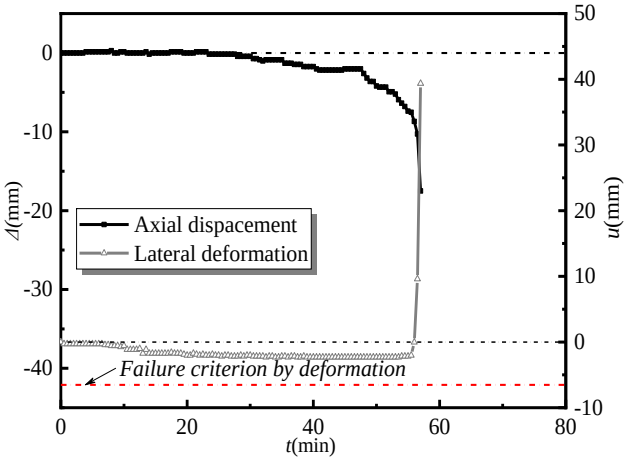

(d) CSUP-P80-70-4

Fig.16 Deformation histories of circular SRCFST specimens

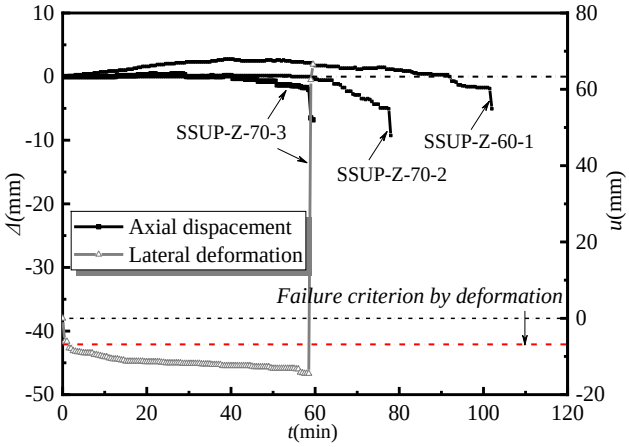

(a)

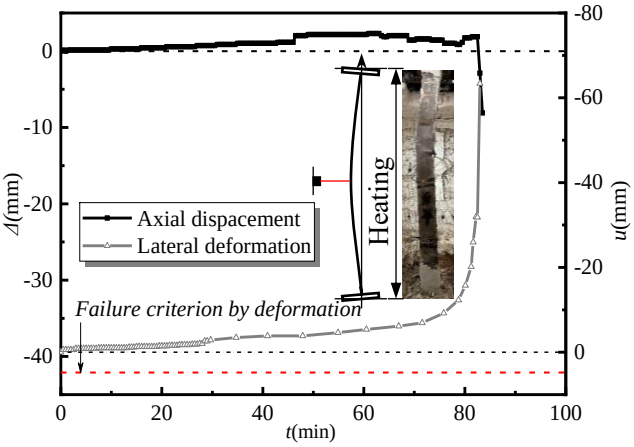

(b)

Fig.17 Deformation versus time relationships of square SRCFST column specimens (a) Deformation readings of specimens SSUP-Z-6-1, SSUP-Z-70-2 and SSUP-Z-80-3; (b) Deformation versus time relationships of SSUP-Z-80-4

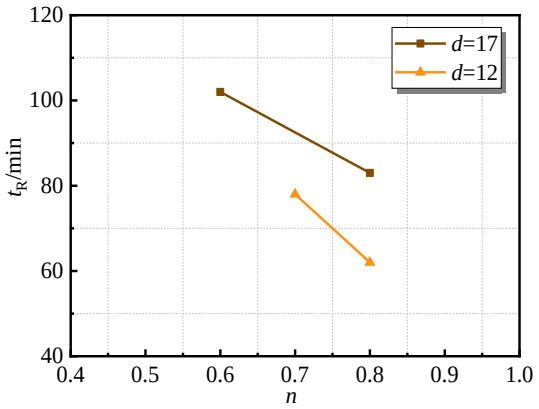

Fig.18 Influence of load level on fire resistance

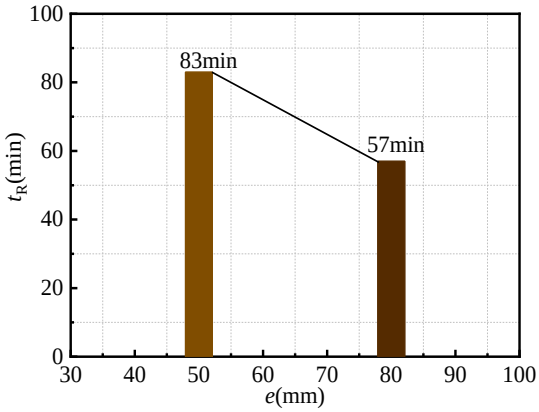

Fig.19 Influence of eccentricity on fire resistance

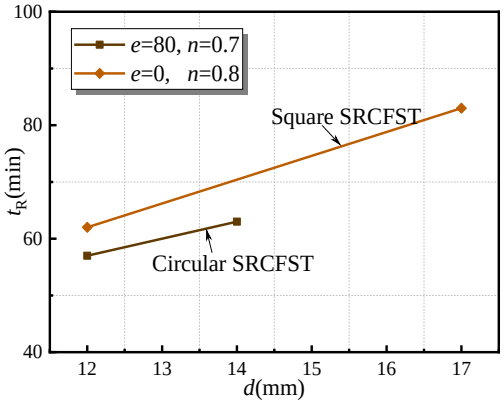

Fig.20 Influence of thickness of the protection material

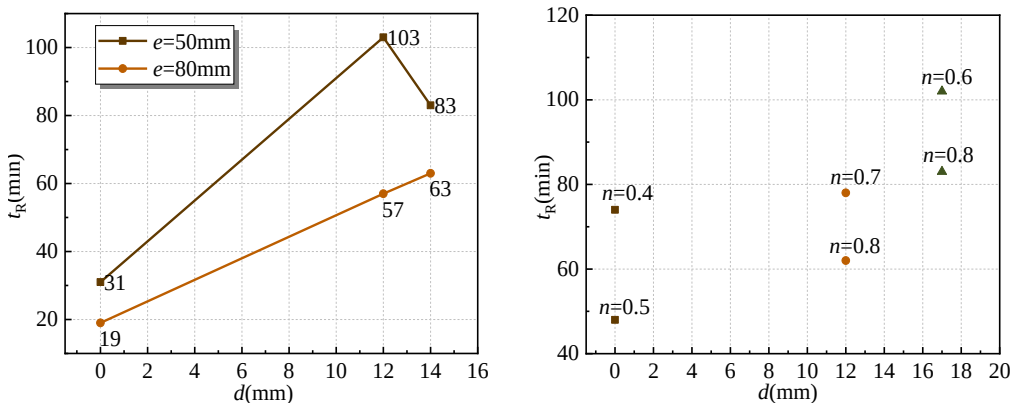

(a) Circular SRCFST column specimens (b) Square SRCFST column specimens

Fig.21 Influence of the fire resistive coating on fire resistance

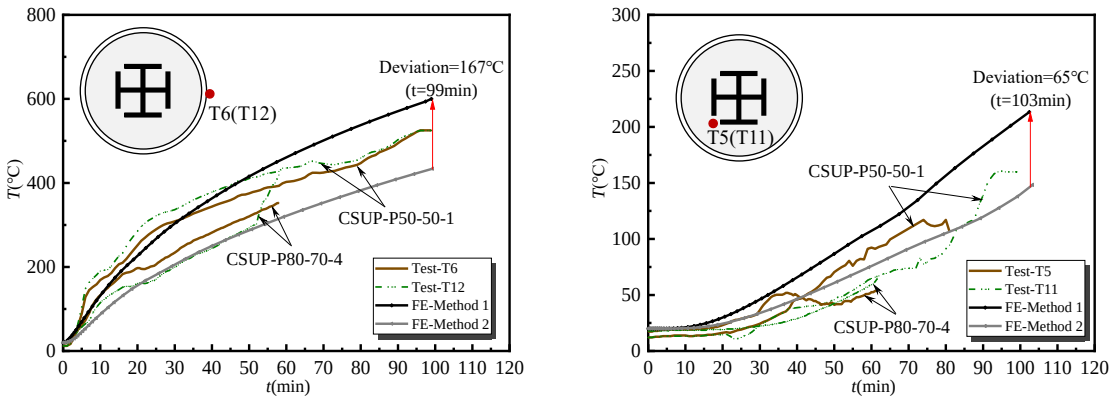

(a) Steel tube (b) Concrete

Fig.22 Influence of thermal resistance of protection material on temperature development

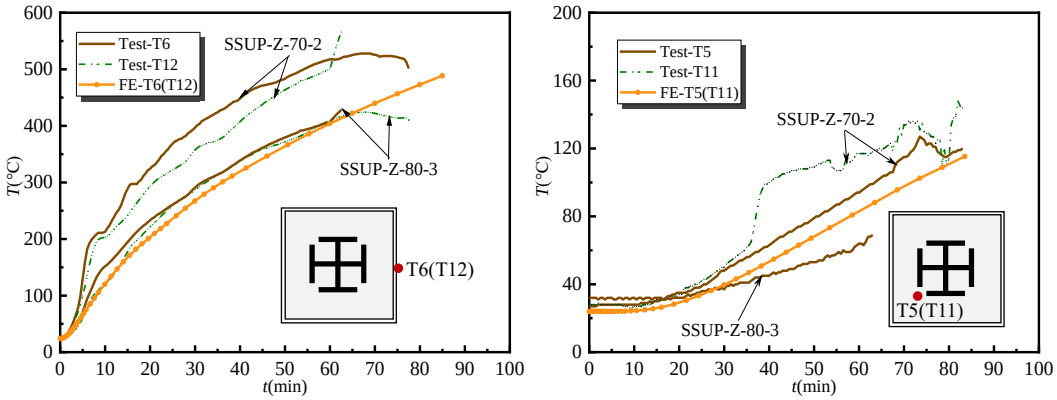

(a) Steel tube (b) Concrete

Fig.23 Comparison of measured and predicted temperature obtained by steel tube and concrete

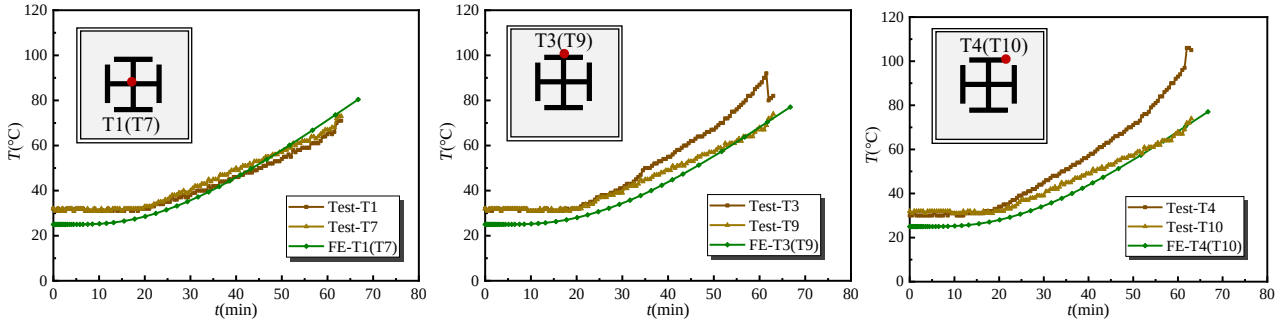

(a) Point T1 and T7 (b) Point T3 and T9 (c) Point T4 and T10

Fig.24 Comparison of measured and predicted temperature obtained by profiled steel (SSUP-Z-80-3)

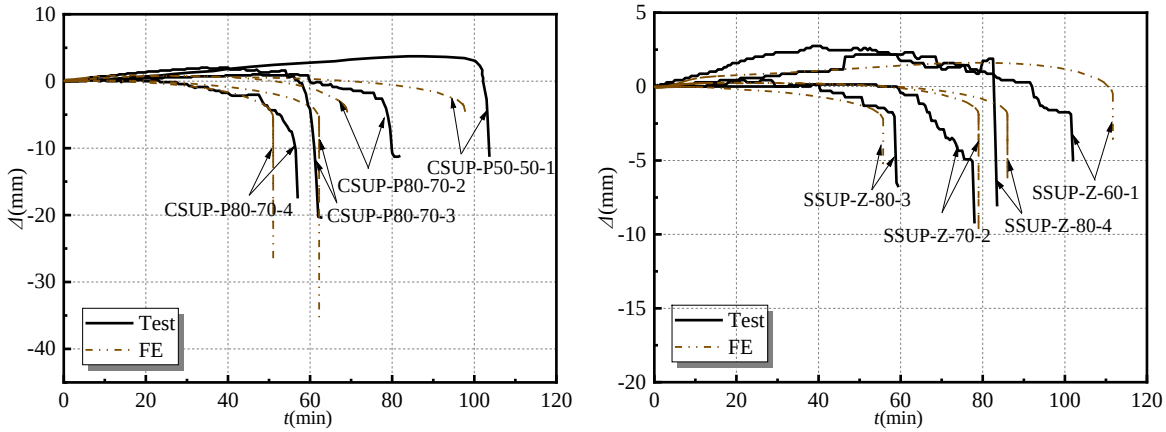

(a) Circular SRCFST column specimens (b) Square SRCFST column specimens

Fig.25 Comparison of measured and predicted axial deformation of protected SRCFST column specimens

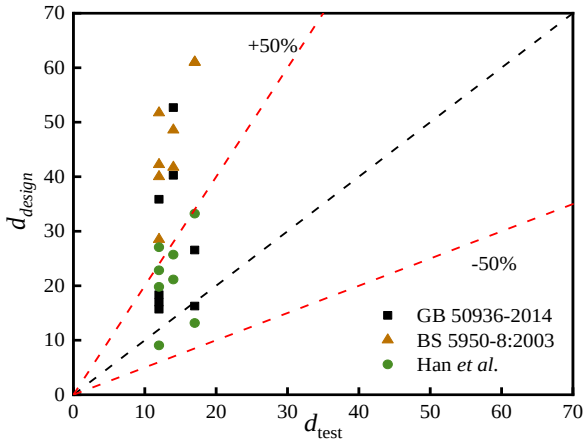

Fig.26 Protection thickness of SRCFST columns predicted by design methods

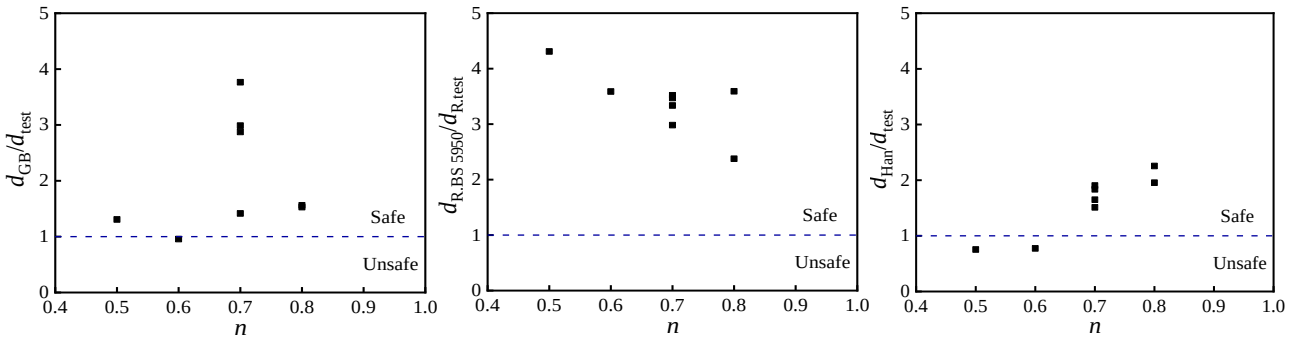

(a) GB 50936-2014 (b) BS 5950-8:2003 (c) Han *et al.*

Fig.27 Predicted and measured protection thickness of SRCFST columns against the load level

Captions for Tables

Table 1 Measured geometric dimensions of SRCFST specimens

Table 2 Material properties of steel

Table 3 Mixture proportions of concrete (relative to weight of cement)

Table 4 Summaries of fire resistance time for unprotected and protected SRCFST columns

Table 5 Comparison of measured and predicted temperature of bare SRCFST column specimens

Table 6 Comparison of FE results and test results

Table 7 Summary of protection thickness for SRCFST columns according to three methods

Captions for Figures

Fig.1 Longitudinal dimensions of specimens (unit: mm)

Fig.2 Cross-sectional dimensions and locations of thermocouples in the cross-section (unit: mm)

Fig.3 Details of test coupons and positions of thermocouples (unit: mm)

Fig.4 Fire furnace

Fig.5 Surface conditions of test coupons before fire test and after fire test

Fig.6 Measured temperature (T) versus time (t) relationships

Fig.7 Details of test setup and position of SRCFST column specimen in fire furnace

Fig.8 The failure mode of CSUP-P50-50-1 after the fire exposure

Fig.9 The failure mode of typical square SRCFST specimens after the fire exposure

Fig.10 Comparison of failure modes for SRCST column specimens after removing the fire resistive coating (West)